Petroleum Science 21 (2024) 1552–1568

Contents lists available at ScienceDirect

Petroleum Science

journal homepage: www.keaipublishing.com/en/journals/petroleum-science

Original Paper

Paleoenvironmental reconstruction and organic matter accumulation of the paleogene shahejie oil shale in the Zhanhua Sag, Bohai Bay Basin, Eastern China

Xiao-Lin Wang [a, b, *], Xiao-Min Zhu [a, b, **], Jin Lai [a, b], Xing-Yue Lin [a, b], Xiang Wang [a, b], Yu-Shan Du [c], Chao Huang [c], Yu-Rui Zhu [c]

[a] State Key Laboratory of Petroleum Resources and Engineering, China University of Petroleum (Beijing), Beijing, 102249, China
[b] College of Geosciences, China University of Petroleum (Beijing), Beijing, 102249, China
[c] Shengli Oilfield, SINOPEC, Dongying, 257000, Shandong, China

ARTICLE INFO

Article history:
Received 31 October 2023
Received in revised form
19 December 2023
Accepted 4 March 2024
Available online 7 March 2024

Edited by Jie Hao and Meng-Jiao Zhou

Keywords:
Elemental geochemical
Paleoenvironment
Organic matter accumulation
Paleogene shahejie formation
Zhanhua Sag
Bohai Bay Basin

ABSTRACT

The controlling factors of organic-rich shale accumulation is essential for the exploration and development of shale oil and gas resources. The sedimentary environment plays a vital role in the formation of organic-rich sediments in lacustrine facies. This article unravels the mineralogy, geochemistry, and paleoenvironmental evolution during the deposition of the Paleogene Shahejie Formation (Es_3^L). It discusses the effects of paleoclimate, paleosalinity, paleoredox conditions, paleowater depth, and paleoproductivity on organic matter (OM) enrichment. Finally, the OM enrichment model was established. The results show that the mineralogical compositions are mainly composed of calcite (avg. 40.13%), quartz (avg. 21.64%) and clay minerals (avg. 24.07%), accompanied by dolomite (avg. 7.07%), feldspar (avg. 6.36%) and pyrite (avg. 2.95%). The Es_3^L shale has a high abundance of OM, with total organic carbon (TOC) ranging from 1.07% to 5.12%. The organic matter type is mainly composed of type I-II_1 kerogen, which is generally considered a good-quality source rock. The source of OM is a mixture of lower bacteria, algae, and plants. During the early sedimentary period, the paleoclimate was dry and cold, with high salinity, intense reducibility, and relatively low productivity. During the late sedimentary period, the climate became warmer and more humid. As a result, the salinity decreased to a level that was suitable for biological reproduction, and productivity increased gradually due to the input of terrigenous plants. Paleosalinity and paleoclimate determined the environment of the sedimentary period, in addition, paleoproductivity and paleoredox condition indicated the formation and preservation conditions of OM. The warm and humid climate, brackish water, suitable reduction conditions and high productivity are the favorable conditions for the generation and preservation of organic matter. The research results may have implications for the genetic mechanisms of organic matter accumulation. They will provide theoretical and technical insights into the exploration and development of shale oil.

1. Introduction

The oil shale exploration has become the focused subject in recent years (Hakimi et al., 2019; Zou et al., 2019). Large amounts of shale oil have been produced from the Bakken Formation in the Williston Basin, the Eagle Ford Formation in the western Gulf of Mexico Basin, and the Bone Spring Formation in the Permian Basin (Floyd and Leveridge, 1987; Jones and Manning, 1994; Bhattacharya and Carr, 2019; Nandlal and Weijermars, 2022). These zones are characterized by a high abundance of OM, fluid oil, and ease of production (Reynolds and Umekwe, 2019). Oil shale in China is primarily found in continental lacustrine basins, such as the Yanchang Formation in the Ordos Basin (Fu et al., 2018), the Lucaogou Formation in Jimusar Sag, Junggar Basin (Lai et al., 2022; Hu et al., 2022), the Shahejie Formation in Jiyang Depression, Bohai Bay

* Corresponding author.
** Corresponding author.
E-mail addresses: 2022310023@student.cup.edu.cn (X.-L. Wang), xmzhu@cup.edu.cn (X.-M. Zhu).

https://doi.org/10.1016/j.petsci.2024.03.001

Basin, and Qingshankou Formation in Songliao Basin, as well as other large lacustrine basins (Lai et al., 2020; Kong et al., 2020; He et al., 2017; Li et al., 2023; Yang et al., 2023).

In recent years, many researchers have conducted extensive investigations on the paleoenvironment, geochemical characteristics and OM enrichment mechanisms of organic-rich oil shale (Brumsack, 2006; Hakimi et al., 2017; Ertug et al., 2019; Yang et al., 2022). The paleoenvironment can reflect the sedimentary characteristics of oil shale, which is of great significance for the enrichment and exploration of oil shale (Pehlivanli et al., 2014; Rocha et al., 2023). Paleoclimate conditions control the productivity of lake basin, the supply of terrigenous materials and the redox conditions of water (Lerman, 1978). The enrichment of OM is influenced by paleoproductivity and redox conditions as well as the large terrestrial debris input, in addition the high salinity environment of lake basins also has impact on the OM enrichment in lacustrine oil shale (Carroll and Bohacs, 1999; Liang et al., 2018a,b; F. Li et al., 2022).

The Es_3^L Formation in the Zhanhua Sag of the Bohai Bay Basin contains thick layers of organic rich fine-grained sedimentary rocks with an average thickness of 300–500 m (Song et al., 2020). Numerous commercial shale oilfields have been discovered in the Dongying Sag and Zhanhua Sag (Li et al., 2019; Lai et al., 2022). However, most of the previous studies focused on the mineral and lithofacies characteristics of Well L69 in Zhanhua Sag. Few studies have explored the relationship between paleoenvironment and organic matter enrichment. Additionally, large number of published articles solely utilize elemental geochemical methods to investigate paleoenvironmental reconstruction and OM enrichment. Organic geochemical results provide the most favorable evidence for both the source and preservation of organic matter (Peters and Moldowan, 1991; Peters and Cassa, 1994; Peters et al., 2007).

In this study, organic and element geochemistry data are systematically combined to analyze the differences in major, trace elements and biomarkers in sediments to indicate the paleoenvironmental evolution. The factors of OM enrichment are revealed based on the relationship between TOC and various paleoenvironments. Finally, an OM enrichment model for Shahejie Formation oil shale is established. The research above can support geological theory for exploring shale oil in continental lacustrine environments.

2. Geological settings

The Bohai Bay Basin located in the eastern China, and it is a Mesozoic-Cenozoic continental basin developed on a stable Paleozoic basement with pre-Sinian metamorphic rocks (Wang et al., 2015; Ma et al., 2016; Zhu et al., 2022). The Bohai Bay Basin is adjacent to the Ludong Uplift in the east, with the ancient Yanshan fold belt in the north, Luxi Uplift in the south, and Taihang Mountain fold belt in the west (Cao et al., 2014). The total area of the basin is nearly 2×10^5 km^2, with a planar shape similar to a parallelogram (Fig. 1(a)). The Jiyang Depression is a secondary structural unit located in the southeast margin of the Bohai Bay Basin and the west side of the Tanlu fault zone, with a total area of about 2.65×10^4 km^2 (He et al., 2017; Song et al., 2020). Four sags, Dongying, Huimin, Zhanhua, and Chezhen, as well as numerous sub sags, developed from south to north in the depression. Zhanhua Sag, located in the northeast of Jiyang Depression, is a tertiary structural unit of Jiyang Depression in the Bohai Bay Basin, with an area of about 2.8×10^3 km^2 (Ma et al., 2016; Zhu et al., 2022). The Zhanhua Sag is bounded to the north by Chengbei Uplift, to the west by the Yihezhuang Uplift, to the south by Chenjiazhuang Uplift, and to the east by the Kendong Uplift, respectively (Fawad et al., 2022) (Fig. 1(b)). The region has experienced multiple stages of tectonic evolution and complex fault development (Fig. 1(c)).

The strata in Jiyang Depression include Archaeozoic (Ar) to Cenozoic (Kz). Among them, the Archaeozoic (Ar) is the main component of the basement, and the Cenozoic strata is the cap rock of the basin, including the Paleogene, Neogene, and Quaternary. The Paleogene includes the Kongdian Formation (Ek), Shahejie Formation (Es) and Dongying Formation (Ed), the Neogene includes the Guantao Formation (Ng) and Minghuazhen Formation (Nm), and the Quaternary includes the Pingyuan Formation (Q) (Wang et al., 2015). The Eocene Shahejie Formation was divided into four intervals: Es_1, Es_2, Es_3 and Es_4 (Fig. 2). The Es_3 member was further divided into the upper, middle, and lower sub-members. In this study, the main research object formation is Es_3 lower sub-members (Es_3^L), which is the most important source rock, widely distributed in the Jiyang Depression, with a total thickness of 300–500 m. During this period, semi-deep and deep lacustrine facies deposits were widely developed (Zhang et al., 2021; Zhu et al., 2022). To study the evolution of the paleoenvironment and organic matter enrichment during the Es_3^L sedimentary period, the Es_3^L Formation is further divided into two stages according to the difference of lithology and organic matter content: early sedimentary (stage 1) and late sedimentary (stage 2) (Wang et al., 2015; He et al., 2017; Liang et al., 2018a,b).

3. Samples and methods

3.1. Mineralogical analysis

Firstly, the core of Yy1-1vf, Yy1-2vf and Jyc1 wells provided by the XRD analysis was performed on 298 shale samples to research the mineralogical characteristics of the rocks (checkout equipment: D/max-2500PC diffraction instrument). The shale sample particles were ground to less than 40 μm, then analyzed with a X' Pert PRO, MPD X-ray with Cu Kα radiation (40 kV, 40 mA) at a scanning speed of 2°/min and a testing angle range of 5°–85°. Finally, a computer analysis diffraction chart is used to analyze the content of various minerals. To observe the microstructure characteristics of the samples, field emission scanning electron microscopy (FE-SEM) analysis was conducted by Quanta 250 FEG + Inca X-max20 equipment. Before argon ion polishing, the sample is cut to a suitable size (typically 1 mm × 1 mm × 3 mm) and then placed on a baffle to be polished with argon ion beams.

3.2. Rock-eval pyrolysis and organic geochemistry

Organic geochemical characteristics can also provide a favorable basis for hydrocarbon source, sedimentary environmental and oil shale resource evaluation (Peters and Moldowan, 1991). 107 samples of shales were used to analyze TOC and rock pyrolysis. TOC was analyzed using a Leco CS-230 Carbon and Sulfur Analyzer in the Geological Research Institute in Sinopec Shengli Oil Field Company. Shale samples were first crushed to 170–200 mesh (75–90 μm) using an agate mortar, and then powdered samples were placed into 12.5% hydrochloric acid solution to remove inorganic carbon. Finally, the samples were completely dried at 60–80 °C in a drying oven after being washed to neutrality by distilled water. Rock-Eval pyrolysis data was measured using a Rock-Eval 6 equipment on crushed samples. The latter were heated to about 600 °C and free hydrocarbon (S_1), residual hydrocarbon generative potential (S_2)

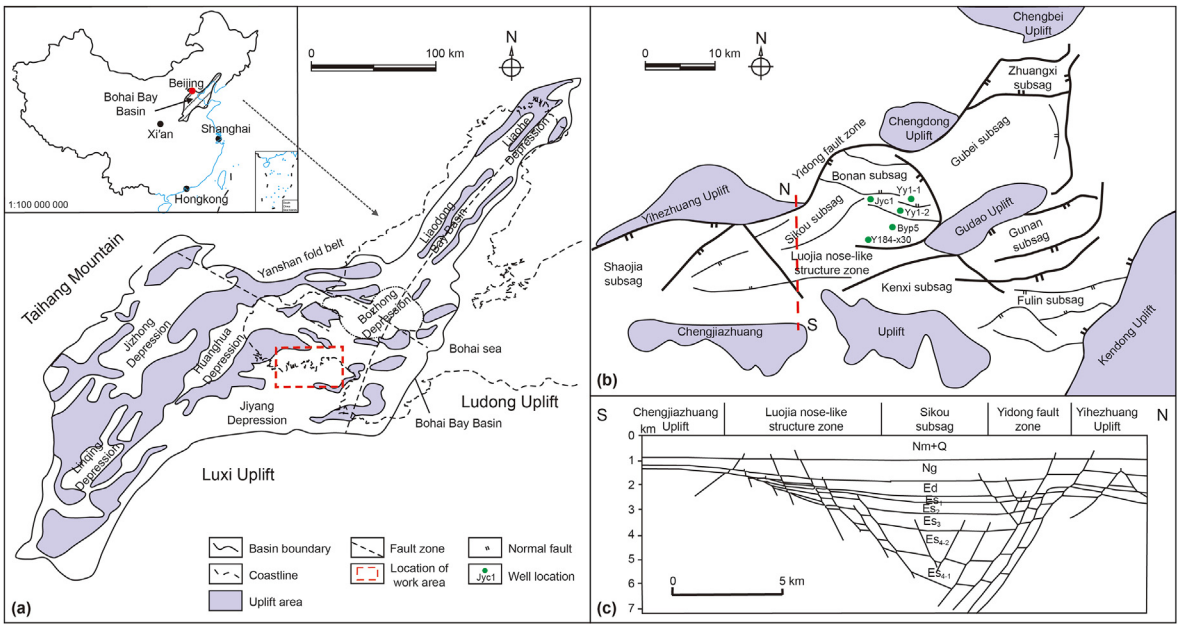

Fig. 1. Geological map of the study area. **(a)** Structural outlines and location of the Bohai Bay Basin. **(b)** Map of the capital tectonic region of Zhanhua Sag. **(c)** Structural profile of the Jiyang Depression (modified after Zhu et al., 2022).

and temperature of maximum pyrolysis yield (T_{max}) were measured. Vitrinite reflectance (R_o) is measured by a microscopic photometer (UMSP-50). Kerogen type is used to identify macerals of kerogen by biological microscopy with the function of transmitted light and reflected fluorescence (Axio Imager. M 2 m Fluorescence microscope), the type index was calculated based on the different weighting coefficients of each maceral to classify the organic matter types. Gas chromatographic (GC) analysis was performed on an Agilent 7890 gas phase analyzer equipped with an elastic quartz capillary column with helium as carrier gas. The experimental equipment of GC-MS is gas chromatoc-mass spectrometer, the chromatographic column is 5% ben methyl siloxane quartz capillary column, with helium as the carrier, the temperature rises from 80 °C to 320 °C at the rate of 3 °C/min and is maintained for 20 min.

3.3. Major and trace elements analysis

Analysis of major and trace elements provides favorable support for restoration of sedimentary environment and enrichment of organic matter. 76 samples form Jyc1 well major and trace elements was completed by Beijing Research Institute of Uranium Geology. The experimental equipment is ICP-MS. Before the determination of major elements, a certain of crushed samples were weighed put it into a clean ceramic crucible and burn it in muffle furnace. Calculate the Loss on ignition. Weigh the lost powder and add anhydrous lithium tetraborate. The lithium fluoride and ammonium nitrate were mixed evenly and put into the fusion machine for melting and casting to make the glass sample, which was then passed through Axios-max. Before the determination of trace elements, a certain amount of powder samples was weighed and heated to 190 °C with hydrofluoric acid and nitric acid, and then digested at a constant temperature for 24 h. After cooling, the samples were taken out and heated to evaporate the excess reagents. After adding 2 mL nitric acid, the excess reagents were evaporated to dry, and then 1 mL nitric acid was added to seal and heated in the oven at 130 °C for 3 h. The analysis accuracy is better than 5% by element XR plasma mass spectrometer.

4. Results

4.1. Mineralogy

According to the core observation, rock slice, XRD and SEM analysis, the Es_3^L shale is mainly composed of carbonate minerals (the average of carbonate minerals in the stage 1 and 2 are 49.34% and 46.30%, respectively). The carbonate content of most samples is greater than 45%. Among them, calcite is the prominent mineral (avg. 40.13%) (Fig. 3), most of them are micrite lamellar or lenticular bodies, and some has mixed with clay minerals and organic matter. Granular morphology includes granular and columnar (Fig. 4(a) and (b)), and calcite recrystallization or columnar calcite vein can also be observed in slices (Fig. 4(c)). Dolomite is less abundant (avg. 7.07%) and occurs within clay mineral matrix as euhedral crystals, including coarse (Fig. 4(d)) and fine dolomite structures (Fig. 4(e)). The felsic minerals include quartz, plagioclase, and K-feldspar (the average of felsic minerals in the stages 1 and 2 are 28.62% and 29.67%, respectively). The average quartz content is 21.64%. Rock slice and SEM show that detrital minerals grains are often dispersed in the argillaceous matrix (Fig. 4(f)), which is often found that quartz particles are filled in illite and smectite mixed layer (Fig. 4(g)). The average content of plagioclase and K-feldspar is 3.94% and 2.42%, respectively. Numbers of K-feldspar dissolution pores are developed (Fig. 4(h)). Clay mineral content ranges from 10.27% to 39.20% (the average of clay minerals in the stages 1 and 2 are 21.79% and 24.04% respectively). The clay mineral is mainly composed of lamellar illite (Fig. 4(j)) and honeycomb structure montmorillonite (Fig. 4(i)), which the sum of which accounts for 90% of the clay content. Kaolinite (avg. 7.5%) and chlorite (avg. 3.5%) are relatively less. Pyrite can be detected from studied samples (avg. 2.95%), and framboidal pyrite grain aggregates are observed in rock slice (Fig. 4(k)). In addition, bioclasts and ostracoda fossils can also be observed in some samples (Fig. 4(l)).

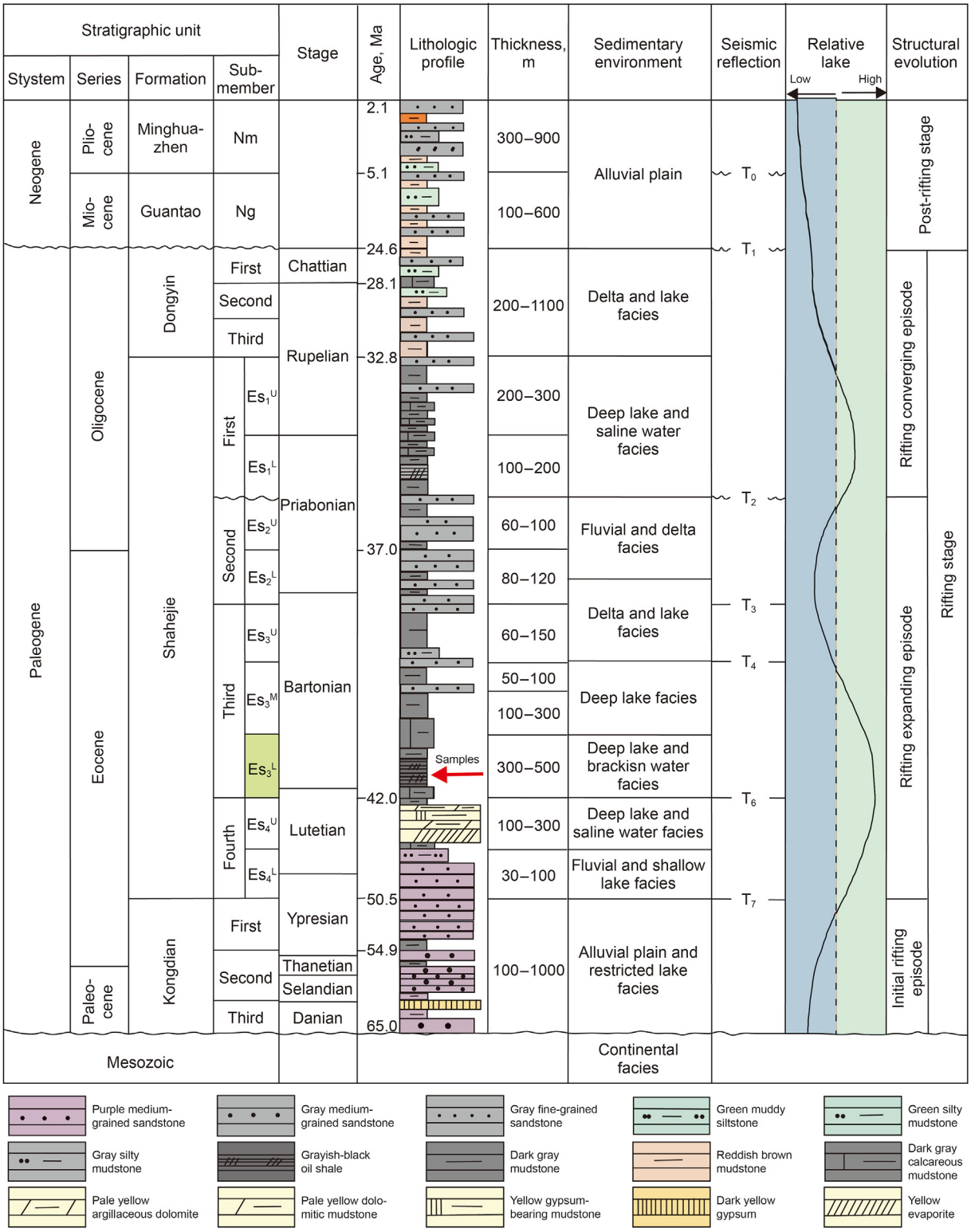

Fig. 2. Stratigraphic column and sequence stratigraphic framework of the Zhanhua Sag, Bohai Bay Basin (modified after Zhu et al. (2005); Jiang et al. (2007)), He et al. (2017)).

4.2. Organic geochemistry

4.2.1. Geochemical characteristics

TOC and rock pyrolysis are common methods to evaluate the abundance and type of organic matter. TOC values of Es_3^L shale samples in the study area ranges from 1.07% to 5.12% (avg. 2.50%). The distribution range of chloroform asphalt "A" was 0.15%–1.26% (avg. 0.48%), which was mainly between 0.2% and 0.6% (Fig. 5(d)). Hydrocarbon generation potential index (S_1+S_2) ranged from 2.16 to 33.74 mg/g (avg. 11.30 mg/g). TOC of stage 1 samples was 1.07%–4.00% (avg. 1.79%). Asphalt chloroform "A" ranges from 0.15% to 0.54% (avg. 0.32%). The hydrocarbon generation potential index

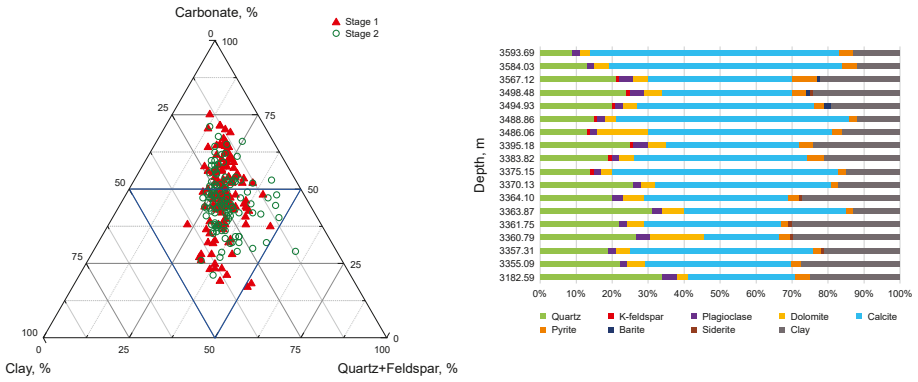

Fig. 3. Ternary plot and bar graphs showing the mineral composition of the Es_3^L shales, Zhanhua Sag, Bohai Bay Basin.

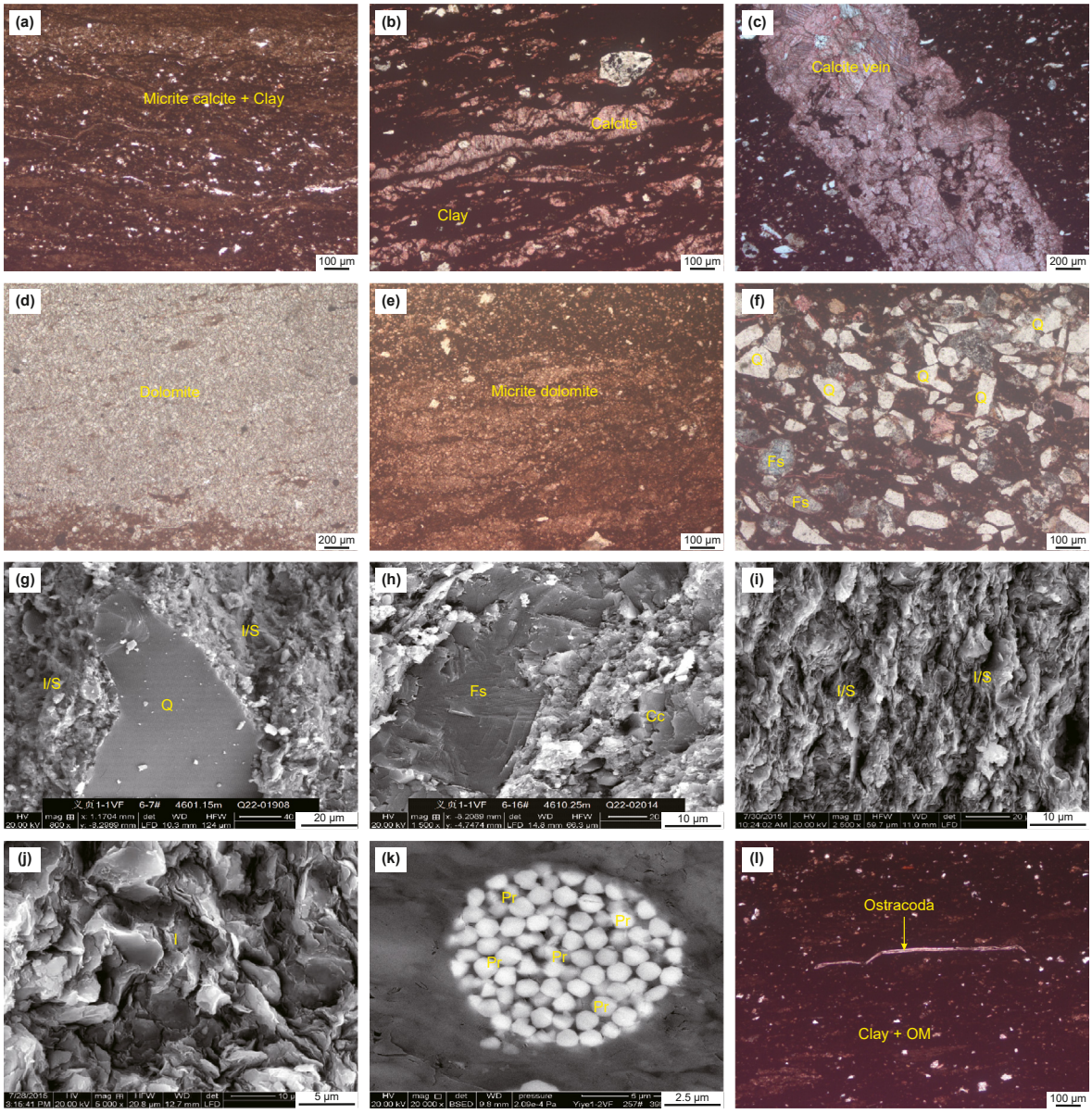

Fig. 4. Microscopic characteristics of the Es_3^L shale, Zhanhua Sag, Bohai Bay Basin. **(a)** Micrite calcite, mixed with mud and organic matter, Yy1-1, 5022.40 m. **(b)** The distribution of calcite and clay material is superimposed, Yy1-1, 4623.30 m. **(c)** Calcite vein, Yy1-1, 5008.20 m. **(d)** Coarse micrite dolomite Yy1-2, 3980.40 m. **(e)** Fine micrite dolomite, Yy1-1, 4600.70 m. **(f)** Clastic minerals such as quartz and feldspar are distributed among clay minerals, Yy1-2, 3974.50 m. **(g)** Quartz minerals are surrounded by clay minerals, Yy1-1, 4601.15 m. **(h)**. Feldspar and calcite corrosion phenomena, Yy1-1, 4610.25 m. **(i)** Honeycomb illite-montmorillonite mixed-layer, Yyc1, 3372.87 m. **(j)** Lamellar illite, Jyc1, 2888.97 m. **(k)** Framboidal pyrite are distributed in groups, Yy1-2, 3927.40 m. **(l)** Ostracoda fossil Yy1-1, 4568.49 m.

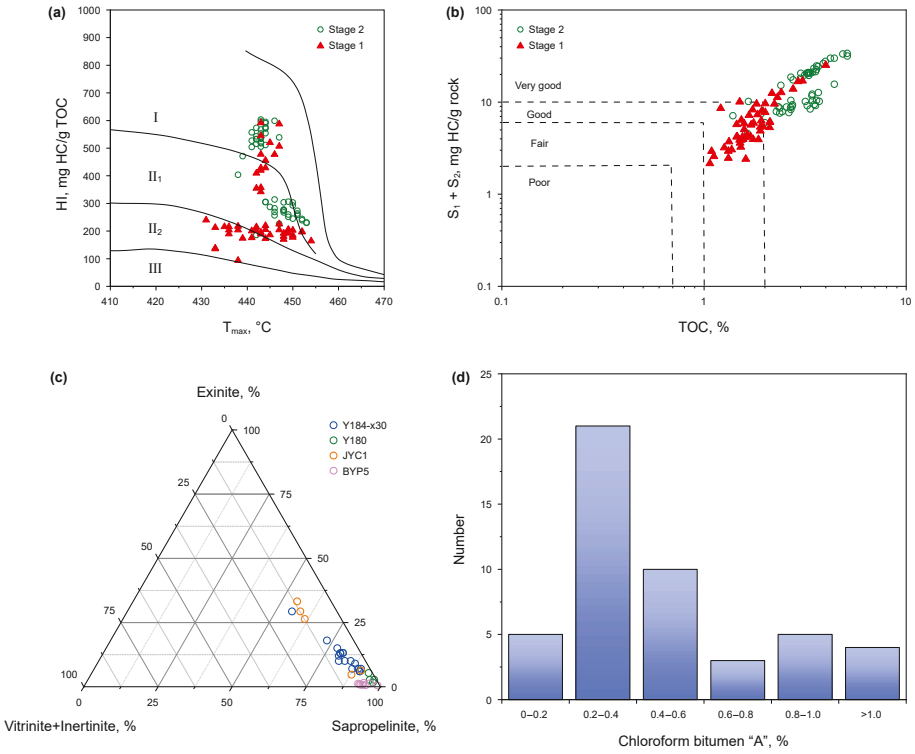

Fig. 5. Basic organic geochemical characteristics of Es_3^L shale, Zhanhua Sag, Bohai Bay Basin. **(a)** The plot of HI-T_{max} indicates the type of organic matter. **(b)** Cross-plot of S_1+S_2 and TOC for determining the quality of source rocks. **(c)** Ternary diagram of kerogen macerals. **(d)** Bar graph showing the distribution of chloroform asphalt "A" values.

(S_1+S_2) was 2.16–25.15 mg/g (avg. 6.62 mg/g). The values of TOC, S_1+S_2, and chloroform asphalt "A" in stage 2 were lower than stage 1 (Table 1). The diagram of S_1+S_2 and TOC is often used to evaluate the potential of OM generation. High quality source rocks have higher S_1+S_2 and TOC values (Espitali'e et al., 1977; Peters, 1986; Langford and Blanc-Valleron, 1990). As can be seen from Fig. 5(b), Es_3^L shale have good hydrocarbon generation potential and the stage 2 is better than stage 1. The diagram of HI-T_{max} shows that the OM types of Es_3^L shale samples are variable, mainly in type I and type II_1 kerogen, and a few samples in stage 1 are distributed in type II_2 kerogen (Fig. 5(a)). Vitrinite reflectance (R_o) ranges from 0.72% to 1.13% (avg. 0.94%), which has generally medium mature (Jin et al., 2021). Kerogen maceral can also be used to identify the type of OM (Ganz and Kalkreuth, 1987; Peters and Cassa, 1994). According to the triangular map of kerogen maceral, OM is generally sapropelic type, ranging from 55 to 98% (avg. 84.6%). Vitrinite and exinite are 0.5%–33% respectively (avg. 9.3%) and between 0.7% and 15.0% (avg. 5.9%) (Fig. 5(c)).

4.2.2. Molecular organic geochemistry

Biomarkers can also be used to analyze the source of organic matter and sedimentary environment (Peters et al., 2007). The characteristics of n-alkanes, isoprenoids, terpane, sterane were characterized by *m/z* 85, *m/z* 191, and *m/z* 217 mass chromatograms.

The distribution and composition of *m/z* 85 n-alkanes are related to the source of organic matter. N-alkanes with high carbon number (usually $>C_{23}$) are mostly evolved products of higher terrestrial plants, while n-alkanes with low carbon number ($<C_{20}$) are usually products of lower aquatic or macrophytes organisms (Czochanska et al., 1988; Peters et al., 2007). The GC of Es_3^L shale samples shows that the carbon number distribution range is from nC_{18} to nC_{28}, the main peak carbon of the samples in stage 1 is mostly nC_{18} or nC_{22}, and the main peak carbon of the samples in stage 2 is nC_{25} (Fig. 7). $\sum nC_{21}^-/\sum nC_{22}^+$ is between 0.28 and 0.88 (avg. 0.53), the average values of the stage 1 and stage 2 ($\sum nC_{21}^-/\sum nC_{22}^+$) are 0.56 and 0.47 respectively. The values of (nC_{21}+nC_{22})/(nC_{28}+ nC_{29}) range from 1.02 to 1.69 (avg. 1.39). Terrigenous/aquatic ratio between stage 1 and stage 2 [TAR = (nC_{27} + nC_{29}+ nC_{31})/(nC_{15} + nC_{17} + nC_{19})] were 0.55–2.61 (avg.1.23) and 1.19–1.59 (avg. 1.37), respectively. Carbon predominance index (CPI) values of stage 1 and stage 2 are 0.77–1.00 (avg 0.86) and 1.10–1.19 (avg 1.15), respectively, odd–even predominance (OEP) values are 0.86–1.03 (avg. 0.92) and 1.17–1.29 (avg. 1.23). The Pr/Ph values of all Es_3^L samples ranged from 0.20 to 1.05 (avg. 0.61), the Pr/Ph values

Table 1
Comparison of TOC and pyrolysis parameters in stage 1 and stage 2, Zhanhua Sag, Bohai Bay Basin.

	TOC, wt%	S_1, mg/g	S_1+S_2, mg/g	T_{max}, °C	Chloroform asphalt "A", %
Stage 2	1.39 ~ 5.12 / 3.18	0.62 ~ 4.56 / 2.27	4.57 ~ 33.74 / 15.82	438 ~ 453 / 446	0.55 ~ 1.26 / 0.91
Stage 1	1.07 ~ 4.00 / 1.79	0.04 ~ 3.40 / 1.01	2.16 ~ 25.15 / 6.62	431 ~ 454 / 443	0.15 ~ 0.54 / 0.32

Note: minimum ~ maximum / average.

of stage 1 and stage 2 ranged from 0.20 to 0.73 (avg. 0.46) and 0.75 to 1.02 (avg. 0.93), respectively, showing strong phytane dominance. Pr/nC_{17} and Ph/nC_{18} can also be used to distinguish the maturity and biodegradation degree of source rocks. Pr/nC_{17} and Ph/nC_{18} values in stages 1 and 2 were 0.11–0.25 (avg. 0.17), 0.19–0.32 (avg. 0.26), 0.40–0.55 (avg. 0.49) and 0.34–0.46 (avg. 0.43), respectively.

Features in Terpane biomarkers can be determined from *m/z* 191 mass chromatograms. C_{30}-αβ-hopane and Ts were highest, with average content of 12.98% and 11.76%, respectively. Ts/(Ts + Tm) values range from 0.45 to 0.93 (avg. 0.75). The gammacerane index (Gammacerane/C_{30} -αβ-hopane) ranged from 0.21 to 0.52 (avg. 0.37).

The *m/z* 217 mass chromatograms showed that the content of diasteranes was lower than regular steranes. C_{27}, C_{28} and C_{29} steranes were the most common steranes series, and the relative abundance of ααα20RC27, ααα20RC28 and ααα20RC29 varied significantly, with the mean mass fraction of 47.21%, 22.97% and 29.83%, respectively. Most of the samples have the distribution characteristics of C27 > C28 < C29. The values of ααα20RC27/ααα20RC29 ranged from 1.08 to 2.37 (avg. 1.63). The C_{28}–C_{29}–C_{30} triangle also reflects the significant contribution of lower plankton and bacteria and algae to the source of OM (Fig. 8) (Peters and Moldowan, 1993; Lai et al., 2022). Maturity biomarker parameters C_{29} sterane ββ/(ββ + αα) values is 0.36–0.58 (avg. 0.47), C_{29} sterane 20 S/(20S + 20R) values is 0.31–0.50 (avg. 0.41) (Fig. 6(a)). This is consistent with the conclusion of OEP-CPI cross-plot analysis of n-alkanes (Fig. 6(b)).

4.3. Elemental geochemical analysis

The major elements measured included Al, Fe, Mg, Ca, Na, K, Mn and Ti, and the trace elements included Cr, V, Co, Cd, Ni, Sr, Ba, Ga, Pb, Zn, B, U and Th. Compared with the Post-Archean Australian shale (PAAS) (Taylor and McLennan, 1985), Ca is obviously enriched in the major elements. The content of Ca in stage 1 was 3.10%–38.36% (avg. 15.68%), and stage 2 is 10.53%–29.91% (avg. 18.52%). The content of Mg and Mn in the stage 1 are 0.61%–5.82% and 0.06%–0.31%, respectively, with an average content of 1.34% and 0.14%. The contents of Mg and Mn in stage 2 are 0.86%–6.41% and 0.04%–0.20%, respectively. The average content was 1.57% and 0.11%. Al, Fe, Na, K and Ti elements are relatively deficient. Among the trace elements, Sr, U and Pb are relatively enriched, among which Sr is the most enriched, with content ranging from 524.2 to 2530 ppm (avg. 1125.2 ppm). The contents of U and Pb elements were 2.18–6.38 ppm (avg. 4.26 ppm) and 7.48–38.49 ppm (avg. 20.39 ppm), respectively. Cr, V, Co, Cd, Ni, Ga, Zn, B, Ba and Th elements are relatively deficient (Fig. 9).

5. Discussion

5.1. Paleoclimate

Paleoclimate controls OM accumulation mainly by influencing the degree of weathering and transformation of unstable materials in sediments (Leythaeuser, 1973). Palynology is considered favorable evidence for paleoclimate (Nowak et al., 2016; Ertug et al., 2019). According to the temperature indication, the spores were divided into three categories: thermophilic, mesothermophilous and cold-tolerant, and divided into xerophytic and hygrophytic according to humidity (Lei et al., 2018). The pollen data of well Y180 showed that from stage 1 to stage 2, the proportion of pollen in the thermophilic and the hygrophytic are gradually increased, the number of pollens in the cold-tolerant and the xerophytic gradually decreased, which also indicated the gradual transformation of the climate from arid and cold to warm and humid in the early to late precipitation period (Fig. 10).

The paleoclimate index "C" can also be used to reflect the paleoclimate conditions (Moradi et al., 2016), value as C = ∑(Fe + Mn + Cr + V + Co + Ni)/∑(Ca + Mg + Sr + Ba + Na + K). Because Fe, Mn, Cr, V, Co, and Ni element tend to be enriched in humid climates, while Ca, Mg, Sr, Ba, Na and K are enriched in arid environments, the higher the "C" value, the wetter the paleoclimate conditions (Hakimi et al., 2017). C-values of 0.6–0.8, 0.4–0.6, and 0.2–0.4 tell of sediment formed under semi-humid, semi-arid to semi-humid, and semi-arid climates, respectively. C-values >0.8 or <0.2 reflect the formation of sediment in a humid or arid paleoclimate environment, respectively (Moradi et al., 2016; Li et al., 2020). The "C value" of Es_3^L samples is 0.22–2.23 (avg. 0.92), stage 1 is 0.29–1.84 (avg. 0.89), stage 2 is 0.22–2.23 (avg. 0.94). It shows that the climate during the early stage of Es_3^L deposition is relatively dry, while the climate is humid and hot in the late stage.

The chemical index of alteration (CIA) is a commonly used measure of chemical weathering. During chemical weathering of upper crust rocks, basic metal elements such as Na, K, and Ca are easily lost from the matrixes and carried away by surface runoff in the form of ions. As a result, the relative abundance of Al_2O_3, which has a more stable chemical composition, gradually increases (Pehlivanli et al., 2014; Moradi et al., 2016). The calculation formula is CIA = 100 × Al_2O_3/(Al_2O_3+CaO*+Na_2O + K_2O), where CaO* is the CaO content incorporated in the silicate fraction (Nesbitt and Young,1982; McLennan et al., 1993; Moradi et al., 2016). A hot, humid climate promotes chemical weathering of rocks, while a cold, dry environment weakens it. CIA values of 50–60, 60–80 and 80–100 reflect the cold-dry, warm-humid, hot-humid paleoclimate, respectively (Nesbitt and Young, 1982; Fedo et al., 1995). The overall CIA value of Es_3^L sample was between 59.58 and 79.08

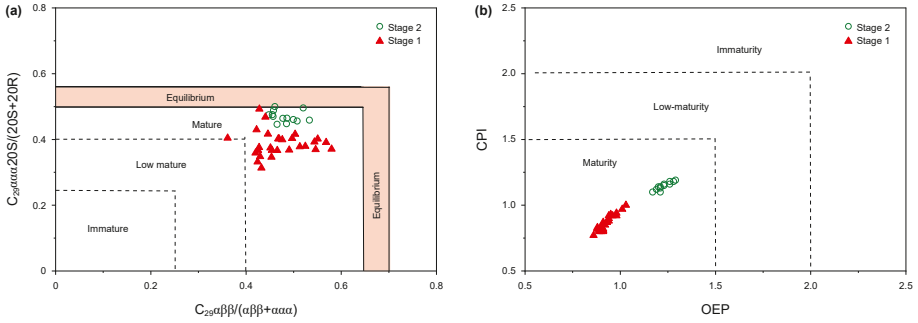

Fig. 6. Discrimination diagrams of maturity by biomarkers of the Es_3^L shale, Zhanhua Sag, Bohai Bay Basin. **(a)** The intersection of C_{29} sterane ββ/(ββ + αα) and C_{29} sterane 20S/(20S + 20R). **(b)** The intersection of OEP and CPI. The evaluation criteria come from Peters and Moldowan (1993).

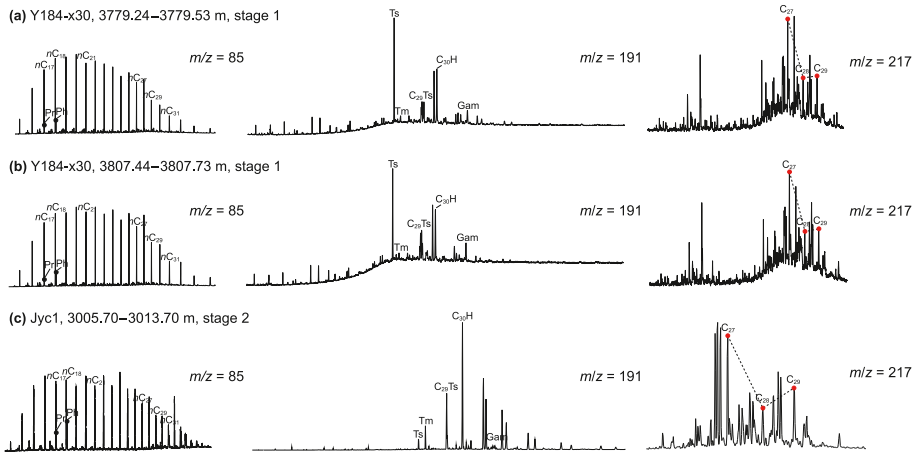

Fig. 7. The *m/z* 191 and *m/z* 217 ion fragmentograms of the saturated fractions showing the distribution of the terpanes and steranes of Es_3^L shale, Zhanhua Sag, Bohai Bay Basin.

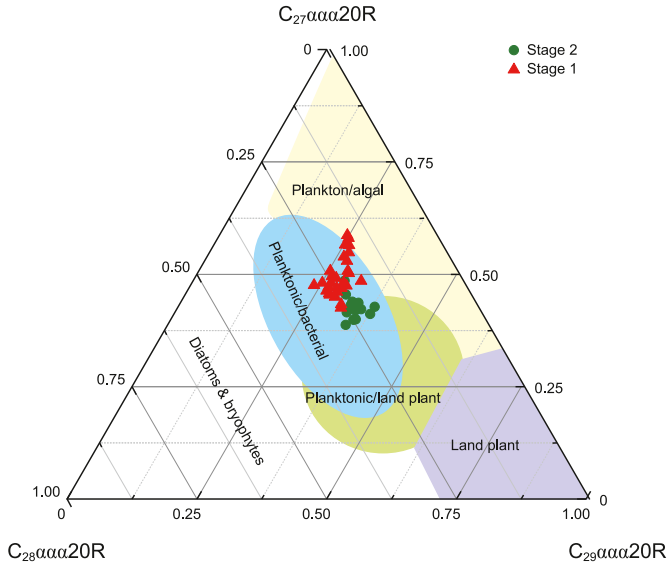

Fig. 8. Ternary diagram of regular steranes (C_{27}, C_{28}, C_{29}) showing the sources of organic matter, Zhanhua Sag, Bohai Bay Basin.

(avg. 73.78), stage 1 is 64.04–79.08 (avg. 73.24), stage 2 is 59.58–79.06 (avg. 74.48). However, due to different degrees of potassium metasomatism occurring in the diagenesis process, resulting in K_2O enrichment in the samples, the CIA calculation result will be low, and thus deviate from the weathering trend, so it is necessary to correct the calculated CIA value (Fedo et al., 1995). The triangular diagram A–CN–K (A = Al_2O_3, CN = CaO*+Na_2O, K = K_2O) can usually be utilized for correction (Fig. 11), and the cross-plot of "C values" and CIA can be judged to reflect warm and humid climate, experiencing moderate chemical weathering (Fig. 12(a)). The results are consistent with the paleoclimate of the study area as determined by the Ga/Rb and K_2O/Al_2O_3 cross plot (Fig. 12(b)).

Rb/Sr can also indicate the variation of climate. Because of Rb is usually present in potassium-rich minerals, it is released and quickly adsorbed by potassium-rich clay during chemical weathering, so it has better stability. However, Sr is easily lost during chemical weathering and enters the lacustrine in the form of ions, with poor stability (Li et al., 2019; Zhang et al., 2021). Rb/Sr showed a decreasing trend under warm climate conditions (Moradi et al., 2016; Wang et al., 2020). Rb/Sr > 0.5 and Rb/Sr < 0.5 represent arid and humid climates, respectively (Khan et al., 2022; Yang et al., 2022). Rb/Sr values of Es_3^L ranged from 51.13 × 10^{-4} to 678.48 × 10^{-4} (avg. 198.36 × 10^{-4}), the average values of Rb/Sr of stage 1 and stage 2 were 201.92 × 10^{-4} and 194.20 × 10^{-4}, indicating that the whole system was in a warm and humid environment.

5.2. Paleosalinity

The salinity of sedimentary water is one of the important factors of OM accumulation, which can be evaluated by the ratio of Sr/Ba and B/Ga (Algeo et al., 2011). Sr and Ba element exist in the form of bicarbonates in fresh water bodies. When salinization occurs and

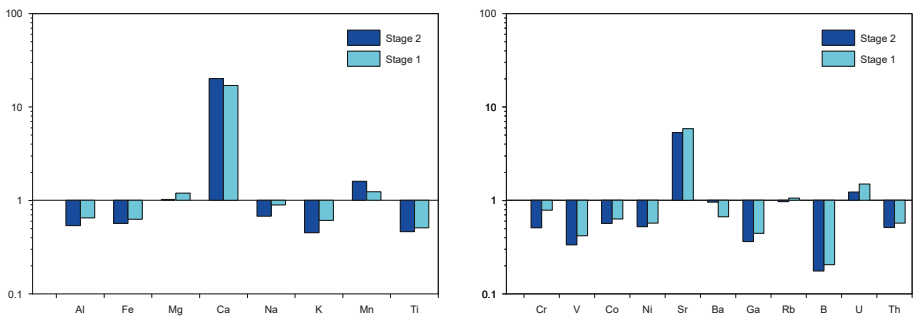

Fig. 9. Enrichment factors of major and trace elements of the Es_3^L samples in comparison to PAAS, Zhanhua Sag, Bohai Bay Basin. Enrichment factors element >1 represents element enrichment, and EF element <1 represents element depletion.

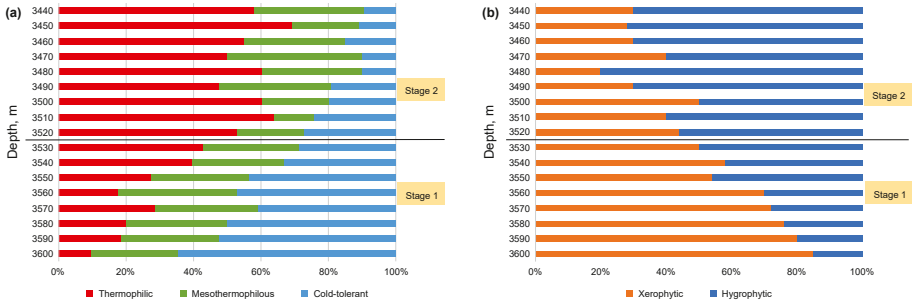

Fig. 10. Pollen climate analysis diagram of Es_3^L shale (well Y180), Zhanhua Sag, Bohai Bay Basin.

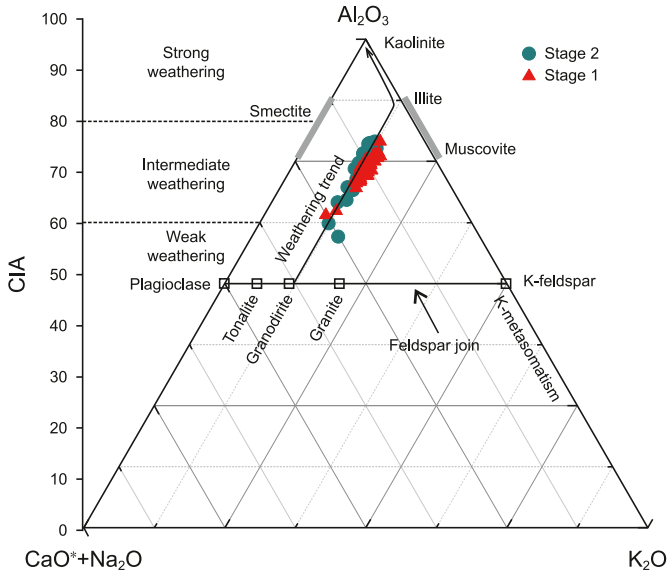

Fig. 11. A–CN–K ternary diagram of Es_3^L shale, Zhanhua Sag, Bohai Bay Basin (Nesbitt and Young, 1982). A = Al_2O_3, CN = CaO*+Na_2O, K = K_2O.

the salinity reaches a certain level, Ba will form $BaSO_4$ precipitation, and the precipitation of Sr begins only when the lacustrine water is continuously salinized. The ratio of Sr/Ba can be used as an indicator of salinity, and high Sr/Ba indicates higher salinity of the sedimentary water bodies (Chivas et al., 1986; Zhang et al., 2019). Sr/Ba >1, <0.6 indicates brackish and fresh water respectively, and 0.6 < Sr/Ba <1 reflects brackish water (Deng et al., 2019; Li et al., 2020). Sr/Ba values ranged from 0.94 to 6.77 (avg. 2.36) of E_{S3}^L shale, indicating a brackish environment. In stage 1 and stage 2, Sr/Ba values ranged from 1.16 to 6.77 (avg. 2.90) and 0.94 to 3.76 (avg. 1.72) (Fig. 13(a)). B/Ga ratio is also often used to discriminate paleosalinity. Ga mainly exists in water in the form of hydroxide, with low solubility and poor migration ability. B/Ga values of freshwater, brackish, and marine water were <3, 3–6, and >6, respectively (Algeo et al., 2011). B/Ga of Es_3^L samples are ranged from 5.14 to 12.66 (avg. 8.22). The B/Ga of stage 1 ranges from 6.03 to 12.66 (avg. 9.34) and stage 2 ranges from 5.14 to 10.67 (avg. 7.28). Indicating that the water salinity in the early stage of sedimentation is saltier than late stage (Fig. 13(b)). In addition, the content of Ca/(Fe + Ca) can also represent salinity of water body. Ca/(Fe + Ca) < 0.4, 0.4–0.8, >0.8 represent freshwater, brackish water, and marine water environment respectively (Lin et al., 2015; Xu et al., 2021). Ca/(Fe + Ca) values of Es_3^L shale in the study area range from 0.48 to 0.97 (avg. 0.83).

The biomarkers of organic geochemistry record sedimentary organic matter and water environment information. Gammacerane is mostly thought to come from salt-like protists. High gammacerane index (gammacerane/C_{30}hopane >0.1) indicates the development of anoxic stratification in lacustrine water column under salinity changes (Moldowan et al., 1985; Sinninghe Damst'e et al., 1995; Liu et al., 2017). In general, the gammacerane index rise as the salinity of the sedimentary water increases (Summons et al., 2008; Wang et al., 2022a,b). The gammacerane index of Es_3^L samples are generally high, ranging from 0.14 to 0.52 (avg. 0.35). The gammacerane index in stage 1 ranges from 0.21 to 0.52 (avg. 0.40), and the gammacerane index in stage 2 ranges from 0.14 to 0.35 (avg. 0.26). The above characteristics indicate that the salinity of water in stage 1 is higher than stage 2.

5.3. Paleoredox condition

Paleoredox conditions are the key factors determining the preservation of OM, including mineral composition and

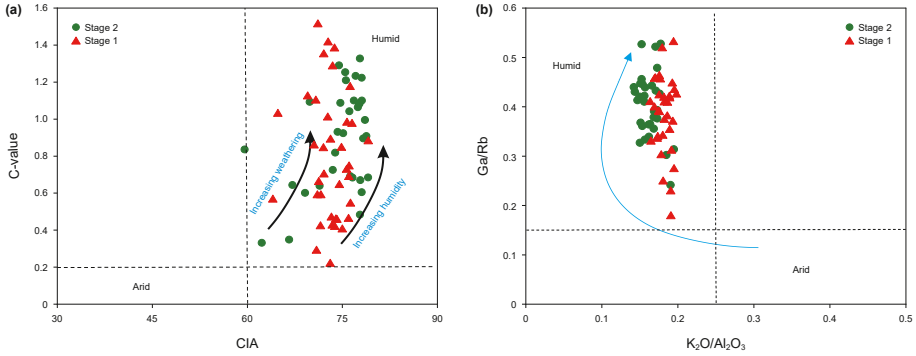

Fig. 12. Paleoclimate analysis of Es_3^L shales, Zhanhua Sag, Bohai Bay Basin. **(a)** Relationship between CIA and C-values. **(b)** The plot of K_2O/Al_2O_3–Ga/Rb. Baseline references from Nesbitt and Young (1982), Roy and Roser (2013).

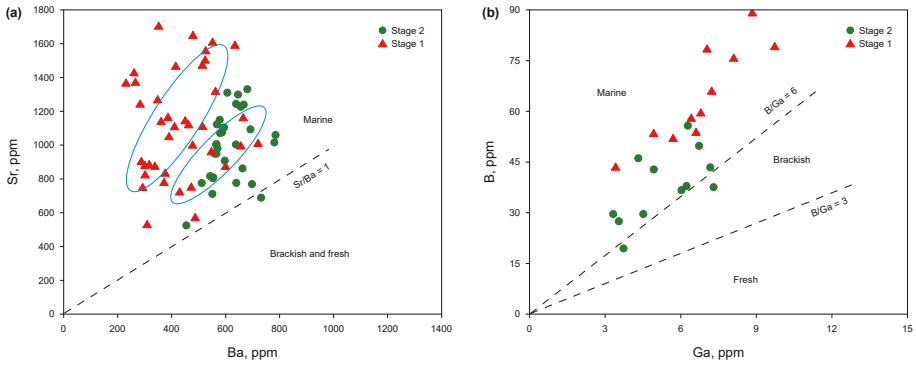

Fig. 13. Cross-plot of Sr/Ba and B/Ga values showing the paleosalinity of Es_3^L shale, Zhanhua Sag, Bohai Bay Basin. **(a)** Relationship between Sr and Ba. **(b)** Relationship between B and Ga.

geochemical characteristics (Aplin and Macquaker, 2011). Pristane (Pr) and phytane (Ph) are products of phytol formed under oxidative and reductive conditions, respectively, the ratio of Pr/Ph is often used to indicate redox conditions (Peters et al., 2007; Wang et al., 2022a,b). Pr/Ph value > 3 indicates oxic conditions, Pr/Ph value between 1 and 3 indicates dyoxic conditions, Pr/Ph value < 1 indicates anoxic conditions (Didyk et al., 1978; Ten Haven et al., 1987). The Pr/Ph values of Es_3^L shale samples are low, ranging from 0.20 to 1.05 (avg. 0.62), indicating anoxic environment. The Pr/Ph values of stage 1 and stage 2 ranged from 0.20 to 0.73 (avg. 0.45) and 0.75 to 1.05 (avg. 0.93), respectively. In addition, the Pr/nC_{17} and Ph/nC_{18} cross-plots provide a method to assess redox conditions and sources of OM (Shanmugam, 1985). As can be seen from the cross-plots, the Es_3^L shale are in a reducing condition. The samples in stage 1 are distributed in the reducing environment area with algal marine organisms as the main source, while the shale samples in stage 2 are mainly distributed in the mixed OM sources and the transitional region of oxidizing and reducing (Fig. 14).

U, Th, V, Ni, Cr, Co, and Mo element are also considered to be redox sensitive trace elements (Crusius et al., 1996; Dean et al., 1997). Paleoredox conditions can use the ratio of V/Cr, Ni/Co, Th/U, δU (δU = U/[1/2(U + Th/3)] and V/(V + Ni) to assess (Hatch and Leventhal, 1992; Jones and Manning, 1994; Wignall and Twitchett, 1996; Zhang et al., 2021). Due to the active nature of uranium, it is easily oxidized and leached, and has strong migration ability. In contrast, thorium is an inert element with weak migration ability.

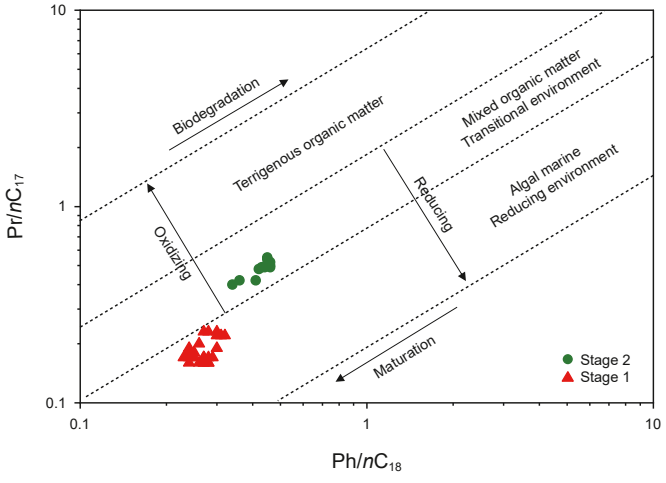

Fig. 14. Cross-plot of Pr/nC_{17} vs Ph/nC_{18}, Zhanhua Sag, Bohai Bay Basin (according to Zhang et al., 2019).

Therefore, the Th/U value and δU can be used to judge the redox state of the sedimentary environment. Anoxic condition δU > 1, oxic condition δU < 1 (Jones and Manning, 1994; Wignall and Twitchett, 1996; Kimura and Watanabe, 2001; Guo et al., 2007). Es_3^L samples have a range of δU values between 0.97 and 1.58, with almost all values greater than 1 (avg. 1.23). The average values for stage 1 and stage 2 are 1.25 and 1.20, respectively. A Th/U ratio greater than 8 indicates an oxic environment, while a ratio less than 2 indicates an anoxic environment. A ratio between 2 and 8 indicates a dyoxic environment (Wignall and Twitchett, 1996). The Th/U ratio of all Es_3^L samples was between 0.79 and 3.18 (avg. 1.92), which the shales were in anoxic-dyoxic environment. The average Th/U ratio of stage 1 and stage 2 was 1.83 and 1.98, respectively. The ratios of V/(V + Ni) > 0.6, 0.46–0.6, <0.46 respectively indicate anoxic, dyoxic and oxic conditions (Hatch and Leventhal, 1992; Jones and Manning, 1994). The overall V/(V + Ni) of Es_3^L shale ranges from 0.22 to 0.80 (avg. 0.63), which is in the dyoxic-anoxic condition.

In lacustrine environments, some trace elements such as Cr and Co are susceptible to terrigenous detrital input and diagenetic processes, V/Cr and Ni/Co ratios may misjudge the true redox conditions (Hatch and Leventhal, 1992; Xiong et al., 2010). V/Cr > 2.0 and Ni/Co > 5.0 indicate dyoxic/suboxic conditions. In the study area, the V/Cr ratio was between 0.43 and 1.52 (avg. 0.83) and the Ni/Co ratio was between 1.33 and 9.19 (avg. 2.70), both of which were lower than the limit of dyoxic conditions. This may be due to the existence of siderite, which led to the low ratio of V/Cr and Ni/Co (He et al., 2017). Therefore, Th/U, δU, V/(V + Ni) and Pr/Ph values were more suitable parameter for determining redox conditions in this study area (Fig. 15(a) and (b)).

5.4. Paleowater depth

Paleowater depth has a significant control effect on the preservation of organic matter. Generally, the greater the water depth, the more conducive to the preservation of organic matter (Zhang et al., 2018; Rimmer, 2004).

Fe is relatively easy to oxidize and has low stability, while Mn can exist stably in solution and be transported for a long distance. Mn/Fe and Fe/Co ratios are usually used to reflect the distance of transportation, which indirectly shows the depth of the water (Yang et al., 2013). A higher Mn/Fe and a lower Fe/Co ratio indicate deeper water (Zhang et al., 2018). The mean values of Mn/Fe in stage 1 and stage 2 were 376.67 × 10^{-4} and 514.29 × 10^{-4}, respectively. The average values of Fe/Co in stage 1 and stage 2 were 275.40 × 10^{-4} and 261.98 × 10^{-4}, respectively, indicating that the water body gradually became deeper during the sedimentary period (Fig. 16(a)). (Al + Fe)/(Ca + Mg) can also represent

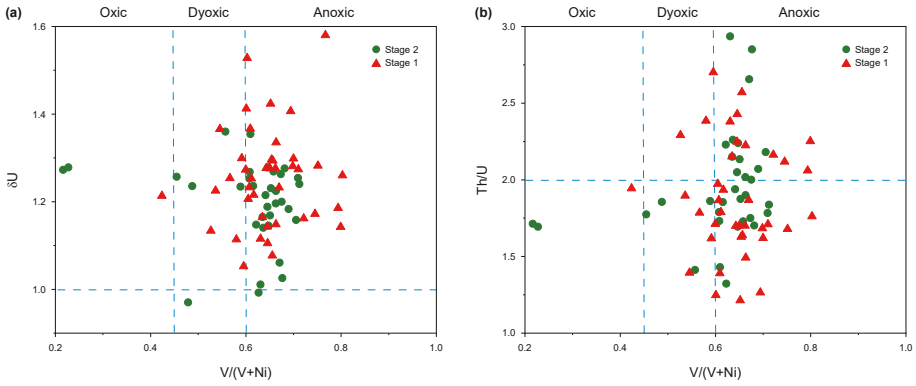

Fig. 15. Characterization of cross-plots of redox proxies in the Es_3^L shale, Zhanhua Sag, Bohai Bay Basin. **(a)** δU vs V/(V + Ni). **(b)** Th/U vs V/(V + Ni).

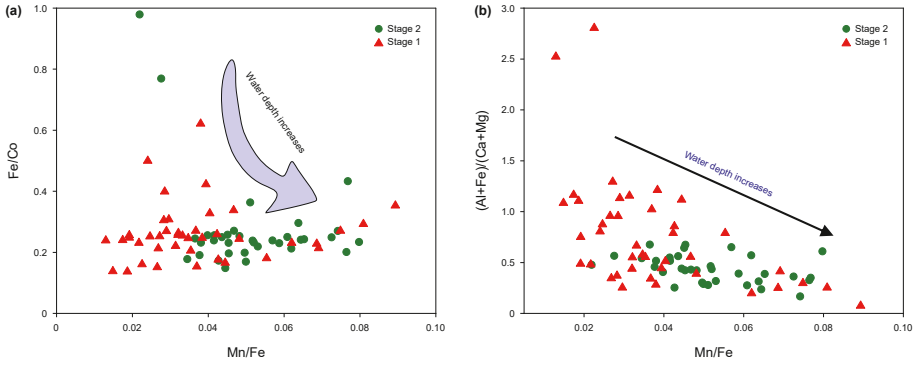

Fig. 16. Characterization of cross-plots of water depth of the Es_3^L shale, Zhanhua Sag, Bohai Bay Basin. **(a)** Fe/Co vs Mn/Fe. **(b)** (Al + Fe)/(Ca + Mg) vs Mn/Fe.

paleowater depth. Fe, Al, Mg, Ca, and other elements in continental sediments mainly come from matrixes efflorescence. Fe and Al are easy to combine with oxygen ions and precipitate in shallow coastal waters, while Mg and Ca are usually enriched in the lacustrine basin on the far shore. Therefore, the (Al + Fe)/(Ca + Mg) ratio in near shore and shallow water environment is significantly higher than that in far shore and deep-water environment (Zhang et al., 2019). The (Al + Fe)/(Ca + Mg) ratio of stage 1 and stage 2 were 0.07–2.80 (avg. 0.76) and 0.17–0.68 (avg. 0.43), respectively. The results were consistent with Mn/Fe and Fe/Co ratios, indicating a process of gradual deepening of water from early to late deposition (Fig. 16(b)).

5.5. Paleoproductivity

During a specific geological period, paleoproductivity refers to the number of organisms produced per unit area and time. A high concentration of OM indicates a high level of paleoproductivity. Terrigenous inputs can be identified by the presence of elements such as Ti and Al (Goldberg and Arrhenius, 1958; Murray and Leinen, 1996). Ti is commonly found in clays and heavy minerals such as rutile and anatase (Kidder et al., 2001). Al is mainly concentrated in clay minerals, feldspar, and other aluminosilicate minerals (Rimmer, 2004). Thus, the Ti/Al ratio can be used to evaluate paleoproductivity (Murray and Leinen, 1996). The Ti/Al ratio of Es_3^L shale ranges from 209.04×10^{-4}–633.11×10^{-4} (avg. 485×10^{-4}), with an average value of 470.01×10^{-4} in the stage 1 and 502.49×10^{-4} in the stage 2, reflecting the paleoproductivity gradually increased. Due to the long residence time and high retention rate of Ba element in seawater, it is an effective index for restoring productivity (Goldberg and Arrhenius, 1958; Dymond et al., 1992). Paleoproductivity can be indicated using biogenic barium (Ba_{bio}) and Ba/Al ratios by excluding the influence of terrigenous detritus (Ganeshram et al., 2000). The formula for calculating Ba_{bio} is $Ba_{bio} = Ba_{sample} - [Al_{sample} \times (Ba/Al)_{PASS}]$, where Ba_{sample} is the total amount of Ba, $(Ba/Al)_{PAAS}$ is the Ba/Al ratio in Post-Archean Australian Shales, and the value is 0.0077 (Taylor and McLennan, 1985; Dymond et al., 1992; Algeo et al., 2011; Dong et al., 2018). Ba_{bio} of stage 1 and stage 2 shale samples are 230.55–719.73 (avg. 434.30) and 454.67–1002.96 (avg. 623.84), respectively. The Ba/Al value is consistent with the Ba_{bio}, reflecting the process of the gradual increase of ancient productivity from early to late period (Fig. 17(a)). The Ba/Al ratio was 33.0×10^{-4}–258.3×10^{-4} ppm (avg. 97.7×10^{-4}), and the average of stage 1 and stage 2 were 71.9×10^{-4} ppm and 128.0×10^{-4} ppm.

Hydrothermal activity affects productivity by altering the redox conditions of the ocean through the presence of hydrothermal fluids containing high concentrations of metallic elements and volatile gases such as CH_4, CO_2 and H_2S (Jones and Gislason, 2008; Y. Li et al., 2022). Hydrothermal activity also provides large amounts of nutrients that promote the growth of algae and other organisms. Previous studies have shown that the ratios of Al/(Al + Fe + Mn) and (Mn + Fe)/Ti (value > 15) can be used to determine the presence of hydrothermal activity during the sedimentary period. Sediments formed solely by hydrothermal activity typically have an Al/(Al + Fe + Mn) value of 0.01. In contrast, sediments of purely biological origin have an Al/(Al + Fe + Mn) value of approximately 0.6, which decreases with increasing hydrothermal

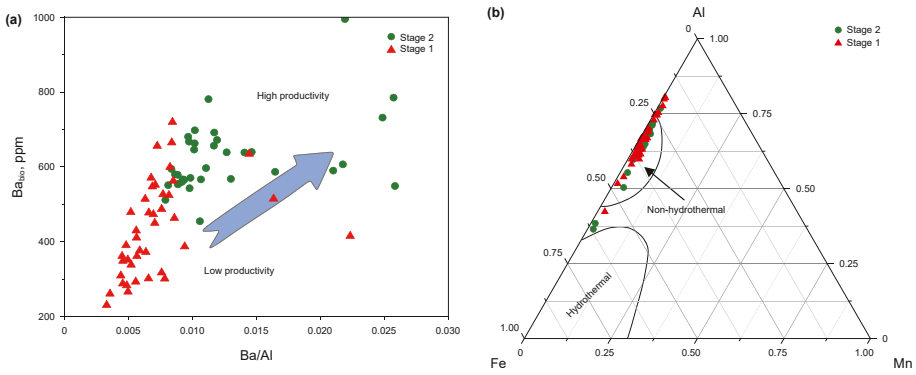

Fig. 17. Characterization of cross-plots of paleoproductivity of the Es_3^L shale, Zhanhua Sag, Bohai Bay Basin. **(a)** Cross-plots of Ba_{bio} and Ba/Al. **(b)** Al–Fe–Mn ternary diagram, modified from Adachi et al. (1986).

activity (Adachi et al., 1986; Yamamoto, 1987). Al/(Al + Fe + Mn) and (Mn + Fe)/Ti values of all Es_3^L samples were 0.37–0.81 (avg. 0.65) and 4.48–76.69 (avg. 12.26), respectively. The Al/(Al + Fe + Mn) values of stage 1 and stage 2 were 0.42–0.81 (avg. 0.66) and 0.36–0.77 (avg. 0.64), respectively. (Mn + Fe)/Ti ratios were 4.48–25.70 (avg. 11.40) and 6.43–76.69 (avg. 13.27). In addition, the Al–Fe–Mn triangle diagram reveals that nearly all sample points fall in the non-hydrothermal region (Fig. 17(b)). This suggests that the study area is largely unaffected by hydrothermal activities. Based on the above indicators, the paleoenvironmental characteristics of the study area from early to late sedimentary period is shown in Table 2.

5.6. Enrichment factors and sedimentary models of organic matter

5.6.1. Organic matter enrichment mechanism

OM enrichment is influenced by many factors in sedimentary environment, including palaeoclimate, paleosalinity, redox conditions, palaeoproductivity and palaeowater depth (Demaison and Moore, 1980; Lash and Blood, 2014). Based on the relationship between TOC and CIA, it is evident that OM increases as the climate becomes warmer and wettest (Fig. 18(a)). Such climate conditions can accelerate atmospheric water circulation, promote the weathering of parent rocks, transport nutrients into the lake, promote organism growth, and lead to an increase in organic matter content and supply. Therefore, warm, and humid climate conditions have a positive effect on OM enrichment. Previous studies have shown that increasing salinity is accompanied by biological flourishing (Pedersen and Calvert, 1990; Liu et al., 2016). However, when the salinity reaches 5‰, the number of organisms is less; when the salinity reaches 15‰, the species and number of organisms reach the highest value, and when the salinity continues to rise to 35‰, the number of organisms gradually decreases (Pedersen and Calvert, 1990; Liu et al., 2016). It can be seen from the cross-plot of TOC value, Sr/Ba and gammacerane index that the samples are overall in saline environment (Sr/Ba > 1 and gammacerane index is high). With the increase of salinity, TOC content gradually decreases (Fig. 18(b) and (c)). Breaching this threshold will result in biological decline. According to the correlation analysis between TOC and the redox condition index (Pr/Ph), TOC and Pr/Ph have different correlation at different stages. Overall, they have a good positive correlation (Fig. 18(d)). The results indicate that the paleoredox conditions have an impact on OM enrichment. A reducing environment is favorable for OM preservation. Based on the relationship between TOC and Fe/Co and Al + Fe/Ca + Mg, there is no clear correlation between paleowater depth and TOC. When the Al + Fe/Ca + Mg value is less than 0.6 and the Fe/Co value is less than 0.25, the TOC value is mainly greater than 3.0. The water depth in stage 2 with high TOC is higher than stage 1 (Fig. 18(e) and (f)). The research indicates that there is a slight increase in the degree of OM enrichment with increasing water depth. The results show that when Ba_{bio} and Al/Ti ratio increase, TOC value exhibits a clear increasing trend. The correlation between Ba_{bio} and TOC is better than that of Al/Ti (Fig. 18(g) and (h)). It can be concluded that higher paleoproductivity leads to a higher degree of OM enrichment.

In summary, the enrichment of OM is the result of the comprehensive influence of multiple factors. Appropriate salinity, warm and humid climate, high productivity and reducing conditions jointly promote the accumulation and preservation of OM. As the climate transitions form dry and cold to warm to humid, precipitation and water depth increase, leading to higher productivity in the water body. During this period, organisms thrive and organic matter is enriched and preserved. Palaeowater depth has the weakest influence on organic matter enrichment compared to other factors.

5.6.2. Organic matter enrichment process and modes

The variation of OM abundance is closely related to paleoenvironment (Fig. 19). The macro environment of sedimentary periods was determined by paleoclimate and paleosalinity. Paleoproductivity and redox conditions indicated the generation and preservation conditions of OM, ultimately controlled the change and accumulation of OM in different sedimentary periods. The specific process is as follows:

During the early stage of Es_3^L deposition (stage 1), the paleoclimate was relatively cold and arid, resulting in little precipitation. The evaporation of a large amount of salt from the lake water led to high salinity and obvious water stratification. There was little provenance supply, resulting in low primary productivity and organic matter content in the sediment (TOC avg. 1.79%).

Table 2
Restoration results of paleoenvironment of the Es_3^L shale, Zhanhua Sag, Bohai Bay Basin.

	Paleoclimate	Paleosalinity	Paleoredox	Paleowater depth	Paleoproductivity
Stage 2	Warm and humid	Moderate	Low reducibility	Deep water	Relatively high
Stage 1	Cold and dry	Very high	High reducibility	Semi-deep water	High

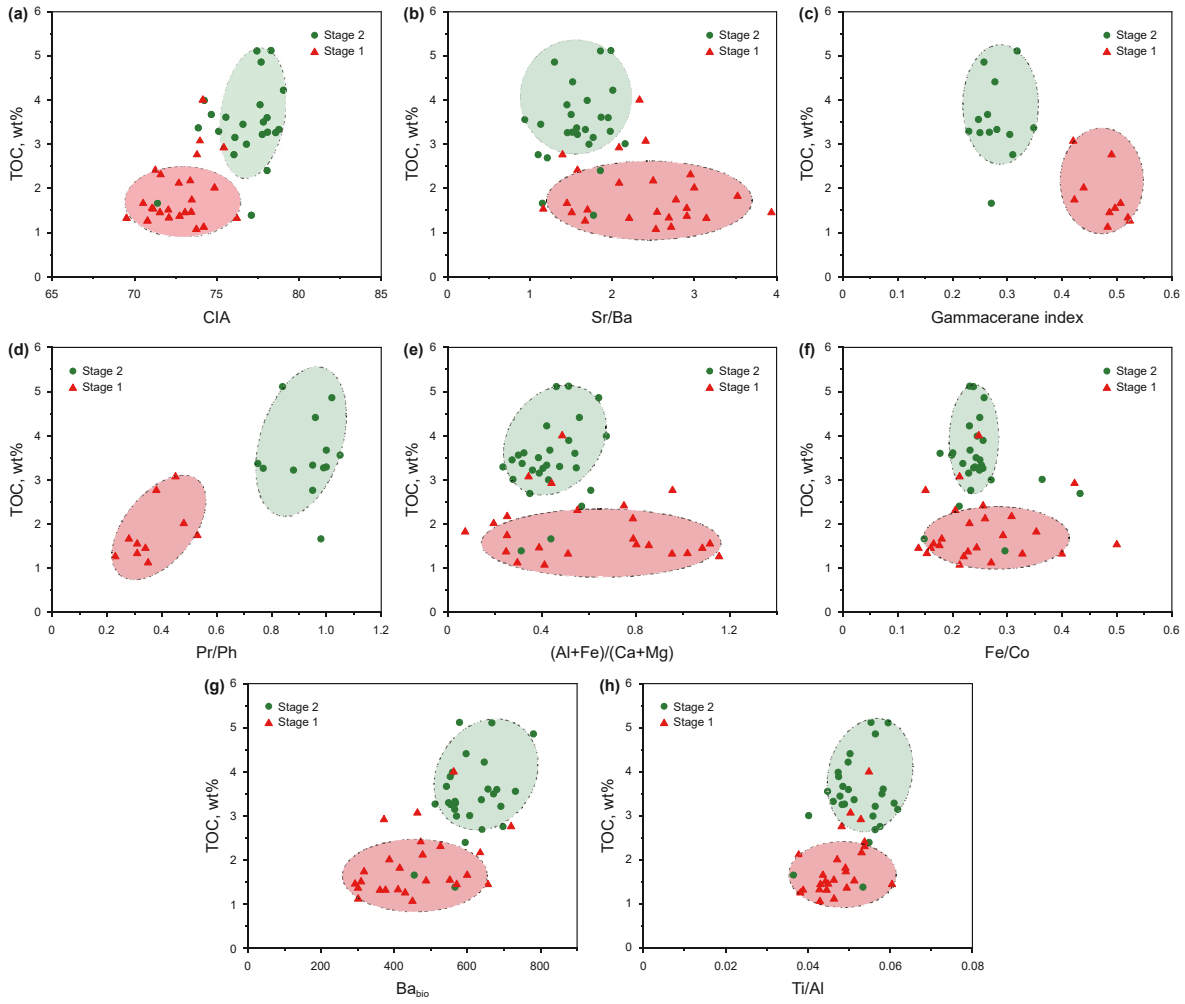

Fig. 18. Cross-plots of TOC and paleoenvironment indicators showing the OM accumulation mechanisms of the Es_3^L shale, Zhanhua Sag, Bohai Bay Basin. **(a)** TOC vs. CIA. **(b)** TOC vs. Sr/Ba. **(c)** TOC vs. gammarerane index. **(d)** TOC vs. Pr/Ph. **(e)** TOC vs. Al + Fe/Ca + Mg. **(f)** TOC vs. Fe/Co. **(g)** TOC vs. Ba_{bio}. **(h)** TOC vs. Ti/Al.

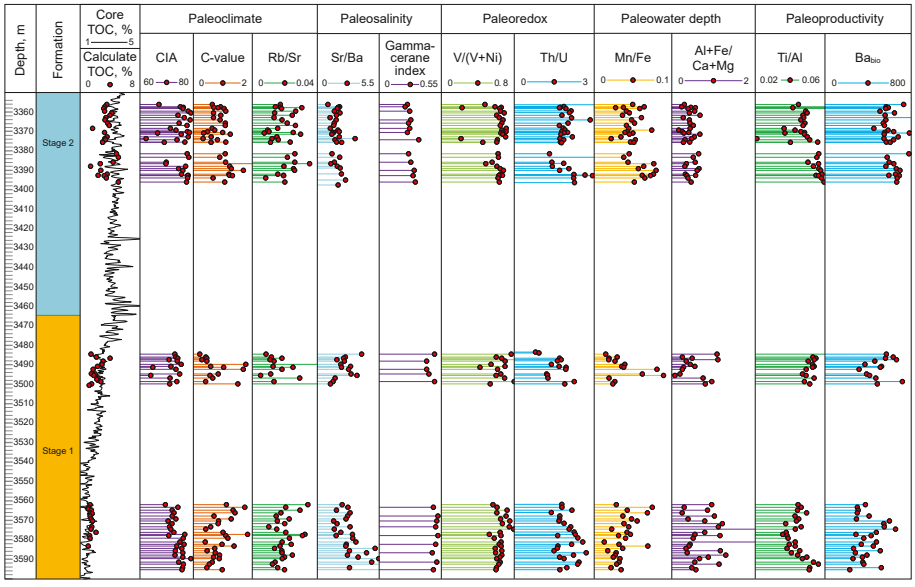

Fig. 19. Vertical stratigraphic alternation of paleoclimate, paleosalinity, paleoredox, paleowater depth and paleoproductivity signals of the Es_3^L shale (well Jyc1), Zhanhua Sag, Bohai Bay Basin.

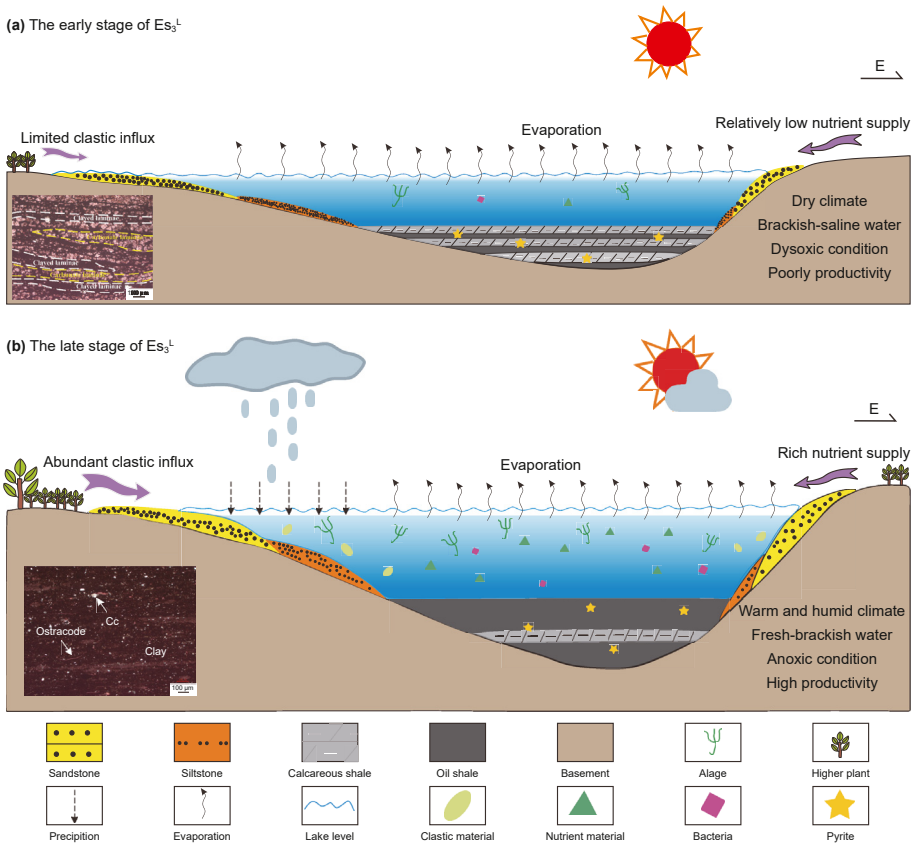

Fig. 20. The environmental evolution and accumulation model of organic matter of Es_3^L Formation, Zhanhua Sag, Bohai Bay Basin.

During the late stage of Es_3^L deposition (stage 2), precipitation increased, causing the water body to deepen rapidly and the climate to gradually warm and become wetter. Debris flowed into the lake, increases the nutrient and providing a good material base for plankton and bacterial algal blooms (Talbot and Kelts, 1990). The paleoproductivity increased, and the respiration and degradation of numbers of organisms consumed the oxygen in the lake water (Kelts and Hsü, 1978), forming reduction conditions to preserve the organic matter, and TOC reached the highest level (avg. 3.18%). Oil shale deposited in reductive environments are generally considered to be reservoirs with high oil generation potential (Didyk et al., 1978; Moldowan et al., 1985; Hatch and Leventhal, 1992). Additionally, numerous studies indicate that optimal conditions for forming high-quality shale oil reservoirs include warm climates, strong terrigenous input, appropriate salinity, and reducing paleoenvironmental conditions (Wang et al., 2015; Zhang et al., 2018; Liang et al., 2018).

Based on the analysis above, sedimentary environment and OM enrichment factors in the study area were comprehensively analyzed according to the characteristics of organic geochemistry and major and trace elements. We established an OM enrichment model for the oil shale in Es_3^L member of the Zhanhua Sag in the Bohai Bay Basin was (Fig. 20). The climate changed gradually from dry and cold to warm and humid from the early stage to the late stage of Es_3^L. The increase of rainfall provided nutrients for lake organisms, resulting in a gradual increase in primary productivity and more suitable water salinity. This created providing favorable conditions for the generation and preservation of OM.

5.6.3. Comparisons with other crucial shales in the Jiyang Depression

Dongying Sag is rich in organic shale and is one of the most promising depressions for shale oil exploration in Jiyang Depression. In the context of the above analysis, this research compares the characteristics of shale in paleoenvironments and mechanisms of organic matter enrichment in the Zhanhua and Dongying Sags.

Numerous scholars have conducted extensive research on the lithofacies, sequence, paleoenvironment, OM enrichment, and sedimentary mechanisms of the shale in Dongying Sag (Cao et al., 2014; Hu et al., 2017; Liang et al., 2018; Lei et al., 2018; Liang et al., 2018a,b; Wu et al., 2022). Shale is primarily composed of carbonate, clay minerals and quartz, TOC is 0.15%–11.4% (avg. 2.27%), mainly formed in medium-depth saline lake sedimentary environment with oxidation limited (Liang et al., 2018; Wu et al., 2022). The sedimentary environment of the lake basin undergoes significant changes, and the paleoclimate has a certain influence on the lake's salinity, terrigenous supply, and biological prosperity, these factors further control the lithofacies and organic matter accumulation (Liang et al., 2018; Liang et al., 2018a,b; Lei et al., 2018). Climate and relative lake surface fluctuations affect algal blooms and terrestrial OM inputs, which in turn affects primary productivity and organic matter production. The accumulation of OM occurs as the result of several inter-connected factors including primary productivity, terrestrial inputs, and variation in oxidizing-reducing conditions (Liang et al., 2018; Liang et al., 2018a,b). To sum up, these factors can either work together, or one can play a leading role. In summary, the mineral composition, sedimentary paleoenvironment, and OM enrichment factors of the shale in Dongying Sag are generally consistent with Zhanhua Sag.

6. Conclusions

(1) The oil shale in the Zhanhua Sag of Bohai Bay Basin is abundant in carbonate minerals, comprising primarily of calcite, quartz, and clay minerals, with minor amounts of dolomite, feldspar, and pyrite.

(2) The Paleogene Es_3^L shale in Zhanhua Sag contains a high abundance of organic matter. The average value of TOC was 2.50%, while the average value of chloroform asphalt "A" was 0.48%, and the mean hydrocarbon generation potential was 11.30 mg/g. The average T_{max} value was 444 °C. The types of organic matter are mainly type I and type II_1 kerogen, with high OM maturity. The sources of OM comprise lower bacteria, algae, and plants.

(3) During the early sedimentary stage, the climate was cold and arid, with intensity evaporation and high salinity, which was not suitable for the growth of most organisms. The paleo-productivity and TOC was relatively low. During the late sedimentary period, the climate gradually became warm and humid, the salinity was more suitable for biological growth. The abundant supply of nutrients higher paleo-productivity, as reflected by high levels of TOC. A warm and humid climate, appropriate salinity, high paleo-productivity, and specific reduction conditions are essential requirements for the generation and occurrence of organic matter.

CRediT authorship contribution statement

Xiao-Lin Wang: Writing – original draft, Validation, Methodology, Investigation, Data curation, Conceptualization. **Xiao-Min Zhu:** Writing – review & editing, Visualization, Supervision, Methodology, Funding acquisition, Conceptualization. **Jin Lai:** Writing – review & editing, Validation, Supervision, Formal analysis, Conceptualization. **Xing-Yue Lin:** Writing – review & editing, Validation, Investigation, Data curation. **Xiang Wang:** Writing – review & editing, Investigation. **Yu-Shan Du:** Resources, Project administration, Funding acquisition. **Chao Huang:** Supervision, Software, Resources, Project administration. **Yu-Rui Zhu:** Validation, Supervision.

Declaration of competing interest

The authors declare that they have no known competing financial interests or personal relationships that could have appeared to influence the work reported in this paper.

Acknowledgments

This work was supported by the National Natural Science Foundation of China (No. 42272110). We are grateful to Sinopec Shengli Oilfield for their support and help in this study. We sincerely appreciate editors and four reviewers, whose comments improved the manuscript.

References

Adachi, M., Yamamoto, K., Sugisaki, R., 1986. Hydrothermal chert and associated siliceous rocks from the northern Pacific their geological significance as indication od ocean ridge activity. Sediment. Geol. 47 (1–2), 125–148. https://doi.org/10.1016/0037-0738(86)90075-8.

Algeo, T.J., Kuwahara, K., Sano, H., Bates, S., Lyons, T., Elswick, E., Maynard, J.B., 2011. Spatial variation in sediment fluxes, redox conditions, and productivity in the Permian–Triassic Panthalassic Ocean. Paleogeogr. Paleoclimatol. Paleoecol. 308 (1–2), 65–83. https://doi.org/10.1016/j.palaeo.2010.07.007.

Aplin, A.C., Macquaker, J.H., 2011. Mudstone diversity: origin and implications for source, seal, and reservoir properties in petroleum systems. AAPG Bull. 95 (12), 2031–2059. https://doi.org/10.1306/03281110162.

Bhattacharya, S., Carr, T.R., 2019. Integrated data-driven 3D shale lithofacies modeling of the Bakken Formation in the Williston basin, North Dakota, United States. J. Pet. Sci. 177, 1072–1086. https://doi.org/10.1016/j.petrol.2019.02.036.

Brumsack, H.J., 2006. The trace metal content of recent organic carbon-rich sediments: implications for Cretaceous black shale formation. Paleogeogr. Paleoclimatol. Paleoecol. 232 (2–4), 334–361. https://doi.org/10.1016/j.palaeo.2005.05.011.

Cao, Y.C., Yuan, G.H., Li, X.Y., Xi, K.L., Wang, X.M., Jia, Z.Z., Yang, T., 2014. Characteristics and origin of abnormally high porosity zones in buried Paleogene clastic reservoirs in the Shengtuo area, Dongying Sag, East China. Petrol. Sci. 11, 346–362. https://doi.org/10.1007/s12182-014-0349-y.

Carroll, A.R., Bohacs, K.M., 1999. Stratigraphic classification of ancient lakes: balancing tectonic and climatic controls. Geology 27 (2), 99–102. https://doi.org/10.1130/0091-7613(1999)027<0099:SCOALB>2.3.CO;2.

Chivas, A.R., De Deckker, P., Shelley, J.M.G., 1986. Magnesium content of non-marine ostracod shells: a new palaeosalinometer and palaeothermometer. Paleogeogr. Paleoclimatol. Paleoecol. 54 (1–4), 43–61. https://doi.org/10.1016/0031-0182(86)90117-3.

Crusius, J., Calvert, S., Pedersen, T., Sage, D., 1996. Rhenium and molybdenum enrichments in sediments as indicators of oxic, suboxic and sulfidic conditions of deposition. Earth Planet Sci. Lett. 145 (1–4), 65–78. https://doi.org/10.1016/S0012-821X(96)00204-X.

Czochanska, Z., Gilbert, T.D., Philp, R.P., Sheppard, C.M., Weston, R.J., Wood, T.A., Woolhouse, A.D., 1988. Geochemical application of sterane and triterpane biomarkers to a description of oils from the Taranaki Basin in New Zealand. Org. Geochem. 12 (2), 123–135. https://doi.org/10.1016/0146-6380(88)90249-5.

Dean, W.E., Gardner, J.V., Piper, D.Z., 1997. Inorganic geochemical indicators of glacial-interglacial changes in productivity and anoxia on the California continental margin. Geochem. Cosmochim. Acta 61 (21), 4507–4518. https://doi.org/10.1016/S0016-7037(97)00237-8.

Demaison, G.J., Moore, G.T., 1980. Anoxic environments and oil source bed genesis. Org. Geochem. 2 (1), 9–31. https://doi.org/10.1016/0146-6380(80)90017-0.

Deng, T., Li, Y., Wang, Z.J., Yu, Q., Dong, S.L., Yan, L., Hu, W.C., Chen, B., 2019. Geochemical characteristics and organic matter enrichment mechanism of black shale in the Upper Triassic Xujiahe Formation in the Sichuan Basin: implications for paleoweathering, provenance and tectonic setting. Mar. Petrol. Geol. 109, 698–716. https://doi.org/10.1016/j.marpetgeo.2019.06.057.

Didyk, B.M., Simoneit, B.R.T., Brassell, S.T., Eglinton, G., 1978. Organic geochemical indicators of palaeoenvironmental conditions of sedimentation. Nature 272, 216–222. https://doi.org/10.1038/272216a0.

Dong, T., Harris, N.B., Ayranci, K., 2018. Relative sea-level cycles and organic matter accumulation in shales of the Middle and Upper Devonian Horn River Group, northeastern British Columbia, Canada: insights into sediment flux, redox conditions, and bioproductivity. Geol. Soc. Am. Bull. 130 (5–6), 859–880. https://doi.org/10.1130/B31851.1.

Dymond, J., Suess, E., Lyle, M., 1992. Barium in deep-sea sediment: a geochemical proxy for paleoproductivity. Paleoceanography 7 (2), 163–181. https://doi.org/10.1029/92PA00181.

Ertug, K., Vecoli, M., İnan, S., 2019. Palynofacies, paleoenvironment and thermal maturity of early silurian shales in Saudi arabia (qusaiba member of qalibah formation). Rev. Palaeobot. Palynol. 270, 8–18. https://doi.org/10.1016/j.revpalbo.2019.06.018.

Espitali'e, J., Laporte, J.L., Madec, M., Marquis, F., Leplat, P., Pauletand, J., Boutefeu, A., 1977. Methode rapide de caracterisation des roches meres, de leur potential petrolier et de leur degre d'evolution. Rev. Inst. Fr. Petrol 32, 23–42. https://doi.org/10.2516/ogst:1977002 (In French).

Fawad, N., Liu, T., Fan, D., Ahmad, Q.A., 2022. Sedimentary facies analysis of the third eocene member of Shahejie Formation in the bonan sag of Bohai Bay Basin (China): implications for facies heterogeneities in sandstone reservoirs. Energies 15 (17), 6168. https://doi.org/10.3390/en15176168.

Fedo, C.M., Nesbitt, H.W., Young, G.M., 1995. Unraveling the effects of potassium metasomatism in sedimentary rocks and paleosols, with implications for paleoweathering conditions and provenance. Geology 23 (10), 921–924. https://doi.org/10.1130/0091-7613(1995)023<0921:UTEOPM>2.3.CO;2.

Floyd, P.A., Leveridge, B.E., 1987. Tectonic environment of the Devonian Gramscatho basin, south Cornwall: framework mode and geochemical evidence from turbiditic sandstones. J. Geol. Soc. 144 (4), 531–542. https://doi.org/10.1144/gsjgs.144.4.0531.

Fu, J.H., Li, S.X., Xu, L.M., Niu, X.B., 2018. Paleo-sedimentary environmental restoration and its significance of chang 7 member of triassic Yanchang Formation in Ordos Basin, NW China. Petrol. Explor. Dev. 45 (6), 998–1008. https://doi.org/10.1016/S1876-3804(18)30104-6.

Ganeshram, R.S., Pedersen, T.F., Calvert, S.E., McNeill, G.W., Fontugne, M.R., 2000. Glacial-interglacial variability in denitrification in the world's oceans: causes and consequences. Paleoceanography 15 (4), 361–376. https://doi.org/10.1029/1999PA000422.

Ganz, H., Kalkreuth, W., 1987. Application of infrared spectroscopy to the classification of kerogen types and the evaluation of source rock and oil shale potentials. Fuel 66 (5), 708–711. https://doi.org/10.1016/0016-2361(87)90285-7.

Goldberg, E.D., Arrhenius, G.O.S., 1958. Chemistry of Pacific pelagic sediments. Geochem. Cosmochim. Acta 13 (2–3), 153–212. https://doi.org/10.1016/0016-7037(58)90046-2.

Guo, Q., Shields, G.A., Liu, C.Q., Strauss, H., Zhu, M.Y., Pi, D.H., Yang, X.L., 2007. Trace element chemostratigraphy of two Ediacaran–Cambrian successions in South

China: implications for organosedimentary metal enrichment and silicification in the early Cambrian. Paleogeogr. Paleoclimatol. Paleoecol. 254 (1–2), 194–216. https://doi.org/10.1016/j.palaeo.2007.03.016.
Hakimi, M.H., Alaug, A.S., Lashin, A.A., Mohialdeen, I.M., Yahya, M.M., Kinawy, M.M., 2019. Geochemical and geological modeling of the Late Jurassic Meem Shale Member in the Al-Jawf sub-basin, Yemen: implications for regional oil and gas exploration. Mar. Petrol. Geol. 105, 313–330. https://doi.org/10.1016/j.marpetgeo.2019.04.030.
Hakimi, M.H., Abdullah, W.H., Makeen, Y.M., Saeed, S.A., Hakame, H.A., Moliki, T.A., Sharabi, K.Q.A., Hatem, B.A., 2017. Geochemical characterization of the Jurassic Amran deposits from Sharab area (SW Yemen): origin of organic matter, paleoenvironmental and paleoclimate conditions during deposition. J. Afr. Earth Sci. 129, 579–595. https://doi.org/10.1016/j.jafrearsci.2017.01.009.
Hatch, J.R., Leventhal, J.S., 1992. Relationship between inferred redox potential of the depositional environment and geochemistry of the upper pennsylvanian (missourian) Stark shale member of the dennis limestone, wabaunsee county, Kansas, USA. Chem. Geol. 99 (1–3), 65–82. https://doi.org/10.1016/0009-2541(92)90031-Y.
He, J.H., Ding, W.L., Jiang, Z.X., Jiu, K., Li, A., Sun, Y.X., 2017. Mineralogical and chemical distribution of the Es_3^L oil shale in the Jiyang Depression, Bohai Bay Basin (E China): implications for paleoenvironmental reconstruction and organic matter accumulation. Mar. Petrol. Geol. 81, 196–219. https://doi.org/10.1016/j.marpetgeo.2017.01.007.
Hu, Q.H., Zhang, Y.X., Meng, X.H., Li, Z., Xie, Z.H., Li, M.W., 2017. Characterization of micro-nano pore networks in shale oil reservoirs of Paleogene Shahejie Formation in Dongying sag of Bohai Bay Basin, east China. Petrol. Explor. Dev. 44 (5), 720–730. https://doi.org/10.1016/S1876-3804(17)30083-6.
Hu, Z.Q., Gao, Z.Q., Liu, Z.B., Jiang, W., Wei, D., Li, Y., 2022. Characteristics of Cambrian tectonic-lithofacies paleogeography in China and the controls on hydrocarbons. J. Pet. Sci. Eng. 214, 110473. https://doi.org/10.1016/j.petrol.2022.110473.
Jiang, Z.X., Chen, D.Z., Qiu, L.W., Liang, H.B., Ma, J., 2007. Source-controlled carbonates in a small Eocene half-graben lake basin (shulu sag) in central hebei province, north China. Sedimentology 54 (2), 265–292. https://doi.org/10.1111/j.1365-3091.2006.00834.x.
Jin, Z.J., Zhu, R.K., Liang, X.P., Shen, Y.Q., 2021. Several issues worthy of attention in current lacustrine shale oil exploration and development. Petrol. Explor. Dev. 48 (6), 1471–1484. https://doi.org/10.1016/S1876-3804(21)60303-8.
Jones, B., Manning, D.A.C., 1994. Comparison of geochemical indices used for the interpretation of palaeoredox conditions in ancient mudstones. Chem. Geol. 111 (1–4), 111–129. https://doi.org/10.1016/0009-2541(94)90085-X.
Jones, M.T., Gislason, S.R., 2008. Rapid releases of metal salts and nutrients following the deposition of volcanic ash into aqueous environments. Geochem. Cosmochim. Acta 72 (15), 3661–3680. https://doi.org/10.1016/j.gca.2008.05.030.
Kelts, K.R., Hsü, K., 1978. Freshwater carbonate sedimentation. In: Lerman, A. (Ed.), Lakes—Chemistry, Geology, Physics. Springer, New York, NY, pp. 295–323.
Khan, D., Liang, C., Qiu, L., Mirza, K., Wang, Y., Kashif, M., Teng, J., 2022. Depositional environment and lithofacies analyses of the Eocene lacustrine shale in the Bohai Bay Basin: insights from mineralogy and elemental geochemistry. Acta Geol. Sin -Engl. Ed. 97 (2), 589–609. https://doi.org/10.1111/1755-6724.14985.
Kidder, D., Xa, L., Erwin, D., Xa, H., 2001. Secular distribution of biogenic silica through the phanerozoic: comparison of Silica-replaced fossils and bedded cherts at the series level. J. Geol. 109 (4), 509–522. https://doi.org/10.1086/320794.
Kimura, H., Watanabe, Y., 2001. Oceanic anoxia at the Precambrian-Cambrian boundary. Geology 29 (11), 995–998. https://doi.org/10.1130/0091-7613(2001)029<0995:OAATPC>2.0.CO;2.
Kong, X.X., Jiang, Z.X., Zheng, Y.H., Xiao, M., Chen, C., Yuan, H., Chen, F.L., Wu, S.Q., Zhang, J.G., Hao, C., Liu, S.Q., 2020. Organic geochemical characteristics and organic matter enrichment of mudstones in an Eocene saline lake, Qianjiang Depression, Hubei Province, China. Mar. Petrol. Geol. 114, 104194. https://doi.org/10.1016/j.marpetgeo.2019.104194.
Lai, J., Fan, X.C., Liu, B.C., Pang, X.J., Zhu, S.F., Xie, W.B., Wang, G.W., 2020. Qualitative and quantitative prediction of diagenetic facies via well logs. Mar. Petrol. Geol. 120, 104486. https://doi.org/10.1016/j.marpetgeo.2020.104486.
Lai, J., Liu, B.C., Li, H.B., Pang, X.J., Liu, S.C., Bao, M., Wang, G.W., 2022. Bedding parallel fractures in fine-grained sedimentary rocks: recognition, formation mechanisms, and prediction using well log. Petrol. Sci. 19 (2), 554–569. https://doi.org/10.1016/j.petsci.2021.10.017.
Langford, F.F., Blanc-Valleron, M.M., 1990. Interpreting Rock-Eval pyrolysis data using graphs of pyrolizable hydrocarbons vs. total organic carbon. AAPG Bull. 74 (6), 799–804. https://doi.org/10.1306/0C9B238F-1710-11D7-8645000102C1865D.
Lash, G.G., Blood, D.R., 2014. Organic matter accumulation, redox, and diagenetic history of the Marcellus Formation, southwestern Pennsylvania, Appalachian basin. Mar. Petrol. Geol. 57, 244–263. https://doi.org/10.1016/j.marpetgeo.2014.06.001.
Lei, H.R., Jiang, Z.X., Zhou, H.K., 2018. Analysis of paleoclimate evolution of the hyperthermal period in the early Paleogen taking the Dongying depression as an example. Earth Sci. Front. 25 (4), 176. https://doi.org/10.13745/j.esf.yx.2017-10-2, 2018.
Lerman, A.D.I., 1978. Lakes: Chemistry, Geology, Physics. Springer, New York, pp. 237–289.
Leythaeuser, D., 1973. Effects of weathering on organic matter in shales. Geochem. Cosmochim. Acta 37 (1), 113–120. https://doi.org/10.1016/0016-7037(73)90249-4.
Li, D.L., Shi, Q.M., Mi, N.Z., Xu, Y., Wang, X.K., Tao, W.X., 2020. The type, origin and preservation of organic matter of the fine-grain sediments in Triassic Yanhe Profile, Ordos Basin, and their relation to paleoenvironment condition. J. Pet. Sci. 188, 106875. https://doi.org/10.1016/j.petrol.2019.106875.
Li, F., Lü, X.X., Chen, J.F., Wang, R., Wang, Y.Y., Chen, Z.Y., 2022. Palaeo-environmental evolution and organic matter enrichment of Eopalaeozoic shales, northwestern Tarim Basin, China: integrated organic and inorganic geochemistry approach. Paleogeogr. Paleoclimatol. Paleoecol. 601, 111123. https://doi.org/10.1016/j.palaeo.2022.111123.
Li, P., Liu, Z.B., Bi, H., Jiang, T., Bian, R.K., Wang, P.W., Shang, X.Y., 2023. Differences in and factors controlling organic matter enrichment in the Ziliujing Formation shale in the Sichuan Basin. Petrol. Sci. https://doi.org/10.1016/j.petsci.2023.10.020.
Li, Y., Wang, Z.S., Gan, Q., Niu, X.L., Xu, W.K., 2019. Paleoenvironmental conditions and organic matter accumulation in upper Paleozoic organic-rich rocks in the east margin of the Ordos Basin, China. Fuel 252, 172–187. https://doi.org/10.1016/j.fuel.2019.04.095.
Li, Y., Zhao, Q.M., Lyu, Q., Xue, Z.J., Cao, X.P., Liu, Z.P., 2022. Evaluation technology and practice of continental shale oil development in China. Petrol. Explor. Dev. 49 (5), 1098–1109. https://doi.org/10.1016/S1876-3804(22)60335-5.
Liang, C., Jiang, Z.X., Cao, Y.C., Wu, J., Wang, Y.S., Hao, F., 2018a. Sedimentary characteristics and origin of lacustrine organic-rich shales in the salinized Eocene Dongying Depression. Geol. Soc. Am. Bull. 130 (1–2), 154–174. https://doi.org/10.1130/B31584.1.
Liang, C., Wu, J., Jiang, Z.X., Cao, Y.C., Song, G.Q., 2018b. Sedimentary environmental controls on petrology and organic matter accumulation in the upper fourth member of the Shahejie Formation (Paleogene, Dongying depression, Bohai Bay Basin, China). Int. J. Coal Geol. 186, 1–13. https://doi.org/10.1016/j.coal.2017.11.016.
Lin, J.F., Hao, F., Hu, H.Y., Tian, J.Q., Wei, D., 2015. Depositional environment and controlling factors of source rock in the Shahejie Formtion of Langgu Sag. Acta Pet. Sin. 36 (2), 163–173. https://doi.org/10.7623/syxb201502004.
Liu, B., Bechtel, A., Sachsenhofer, R.F., Gross, D., Gratzer, R., Chen, X., 2017. Depositional environment of oil shale within the second member of permian lucaogou formation in the santanghu basin, northwest China. Int. J. Coal Geol. 175, 10–25. https://doi.org/10.1016/j.coal.2017.03.011.
Liu, C.L., Li, H.H., Zhang, X., Zheng, S.J., Zhang, L., Guo, Z.Q., Liu, J., Tian, J.X., Zhang, Y., Zeng, X., 2016. Geochemical characteristics of the Paleogene and Neogene saline lacustrine source rocks in the western Qaidam Basin, Northwestern China. Energy Fuels 30 (6), 4537–4549. https://doi.org/10.1021/acs.energyfuels.6b00269.
Ma, Y., Fan, M.J., Lu, Y.C., Liu, H.M., Hao, Y.Q., Xie, Z.H., Liu, Z.H., Li, P., Du, X.B., Hu, H.Y., 2016. Climate-driven paleolimnological change controls lacustrine mudstone depositional process and organic matter accumulation: constraints from lithofacies and geochemical studies in the Zhanhua Sag, eastern China. Int. J. Coal Geol. 167, 103–118. https://doi.org/10.1016/j.coal.2016.09.014.
McLennan, S.M., Hemming, S., McDaniel, D.K., Hanson, G.N., 1993. Geochemical approaches to sedimentation, provenance, and tectonics. Geological society of Ame rica Special Paper 284, 21–40.
Moldowan, J.M., Seifert, W.K., Gallegos, E.J., 1985. Relationship between petroleum composition and depositional environment of petroleum source rocks. AAPG Bull. 69, 1255–1268. https://doi.org/10.1306/AD462BC8-16F7-11D7-8645000102C1865D.
Moradi, A.V., Sarı, A., Akkaya, P., 2016. Geochemistry of the Miocene oil shale (Hançili Formation) in the Çankırı-Çorum Basin, Central Turkey: implications for Paleoclimate conditions, source–area weathering, provenance and tectonic setting. Sediment. Geol. 341, 289–303. https://doi.org/10.1016/j.sedgeo.2016.05.002.
Murray, R.W., Leinen, M., 1996. Scavenged excess aluminum and its relationship to bulk titanium in biogenic sediment from the central equatorial Pacific Ocean. Geochem. Cosmochim. Acta 60 (20), 3869–3878. https://doi.org/10.1016/0016-7037(96)00236-0.
Nandlal, K., Weijermars, R., 2022. Shale well factory model reviewed: Eagle Ford case study. J. Pet. Sci. 212, 110158. https://doi.org/10.1016/j.petrol.2022.110158.
Nesbitt, H.W., Young, G.M., 1982. Early Proterozoic climates and plate motions inferred from major element chemistry of lutites. Nature 299, 715–717. https://doi.org/10.1038/299715a0.
Nowak, H., Servais, T., Pittet, B., Vaucher, R., Akodad, M., Gaines, R.R., Vandenbroucke, T.R., 2016. Palynomorphs of the fezouata shale (lower ordovician, Morocco): age and environmental constraints of the fezouata biota. Paleogeogr. Paleoclimatol. Paleoecol. 460, 62–74. https://doi.org/10.1016/j.palaeo.2016.03.007.
Pedersen, T.F., Calvert, S.E., 1990. Anoxia vs. productivity: what controls the formation of organic-carbon-rich sediments and sedimentary rocks? AAPG Bull. 74 (4), 454–466. https://doi.org/10.1306/0C9B232B-1710-11D7-8645000102C1865D.
Pehlivanli, B.Y., Koç, Ş., Sari, A., 2014. Carbon isotope (δ13C) characteristics of middle Miocene Çayirhan oil shales (Beypazari, Ankara/Turkey): implications on paleoenvironment and paleoclimate. Fuel 135, 427–434. https://doi.org/10.1016/j.fuel.2014.07.012.
Peters, K.E., Cassa, M.R., 1994. Applied Source Rock Geochemistry: Chapter 5: Part II. Essential elements.
Peters, K.E., Moldowan, J.M., 1993. The Biomarker Guide: Interpreting Molecular

Fossils in Petroleum and Ancient Sediments.
Peters, K.E., 1986. Guidelines for evaluating petroleum source rock using programmed pyrolysis. AAPG Bull. 70, 318–329. https://doi.org/10.1306/94885688-1704-11D7-8645000102C1865D.
Peters, K.E., Moldowan, J.M., 1991. Effects of source, thermal maturity, and biodegradation on the distribution and isomerization of homohopanes in petroleum. Org. Geochem. 17 (1), 47–61. https://doi.org/10.1016/0146-6380(91)90039-M.
Peters, K.E., Waters, C.C., Moldowan, J.M., 2007. Biomarkers and Isotopes in Petroleum Exploration and Earth History, the Biomarker Guide.
Reynolds, D.B., Umekwe, M.P., 2019. Shale-oil development prospects: the role of shale-gas in developing shale-oil. Energies 12 (17), 3331. https://doi.org/10.3390/en12173331.
Rimmer, S.M., 2004. Geochemical paleoredox indicators in devonian–mississippian black shales, central appalachian basin (USA). Chem. Geol. 206, 373–391. https://doi.org/10.1016/j.chemgeo.2003.12.029.
Rocha, H.V., Sant'Anna, L.G., Rodrigues, C.F., Mendes, M., Pereira, Z., Lopes, G., de Sousa, M.J.L., 2023. The paleoenvironmental and thermal histories of the Permian Irati Formation shale in the Paraná Basin, Brazil: an integrated approach based on mineralogical and organic imprints. Mar. Petrol. Geol. 154, 106328. https://doi.org/10.1016/j.marpetgeo.2023.106328.
Roy, D.K., Roser, B.P., 2013. Climatic control on the composition of carboniferous-permian gondwana sediments, khalaspir basin, Bangladesh. Gondwana Res. 23 (3), 1163–1171. https://doi.org/10.1016/j.gr.2012.07.006.
Shanmugam, G., 1985. Significance of coniferous rain forests and related organic matter in generating commercial quantities of oil, Gippsland Basin, Australia. AAPG Bull. 69 (8), 1241–1254. https://doi.org/10.1306/AD462BC3-16F7-11D7-8645000102C1865D.
Sinninghe Damste, J.S., Kening, F., Koopmans, M.L., Koster, J., Schouten, S., Hayes, J.M., de Leeuw, J.W., 1995. Evidence for gammacerane as an indicator of water column stratification. Geochem. Cosmochim. Acta 59 (9), 1895–1900. https://doi.org/10.1016/0016-7037(95)00073-9.
Song, M.S., Liu, H.M., Wang, Y., Liu, Y.L., 2020. Enrichment rules and exploration practices of Paleogene shale oil in Jiyang depression, Bohai Bay Basin, China. Petrol. Explor. Dev. 47 (2), 242–253. https://doi.org/10.1016/S1876-3804(20)60043-X.
Summons, R.E., Hope, J.M., Swart, R., Walter, M.R., 2008. Origin of Nama basin bitumen seeps: petroleum derived from a Permian lacustrine source rock traversing southwestern Gondwana. Org. Geochem. 39 (5), 589–607. https://doi.org/10.1016/j.orggeochem.2007.12.002.
Talbot, M.R., Kelts, K., 1990. Palaeolimnological signatures from carbon and oxygen isotopic ratios in carbonates from organic carbon-rich lacustrine sediments. Lacustrine Basin Exploration-Case Studies and modern Analogs. AAPG Mem 1990 (50), 99–112.
Taylor, S.R., McLennan, S.M., 1985. The Continental Crust: its Composition and Evolution. Blackwell Scientific Publication, Oxford, p. 312.
Ten Haven, H.L., Leeuw, J.W. De, Rullkotter, J., Damste, J.S., 1987. Restricted utility of the pristane/phytane ratio as a palaeoenvironmental indicator. Nature 330 (6149), 641–643. https://doi.org/10.1038/330641a0.
Wang, M., Wilkins, R.W., Song, G., Zhang, L.Y., Xu, X.Y., Li, Z., Chen, G.H., 2015. Geochemical and geological characteristics of the Es_3^1 lacustrine shale in the Bonan sag, Bohai Bay Basin, China. Int. J. Coal Geol. 138, 16–29. https://doi.org/10.1016/j.coal.2014.12.007.
Wang, N., Xu, Y.H., Li, W., Wang, F.L., Chen, G., Liu, Y., Cheng, R.J., Liu, H.Q., 2022a. The compositions of biomarkers and macerals in the first member of the Shahejie Formation in the Liaodong Bay subbasin, Bohai Bay Basin: implications for biological sources and seawater incursions. J. Pet. Sci. 218, 110947. https://doi.org/10.1016/j.petrol.2022.110947.
Wang, N., Xu, Y.H., Wang, F.L., Liu, Y., Huang, Q., Huang, X., 2022b. Identification and geochemical significance of unusual C_{24} tetracyclic terpanes in Shahejie Formation source rocks in the Bozhong subbasin, Bohai Bay Basin. Petrol. Sci. 19 (5), 1993–2003. https://doi.org/10.1016/j.petsci.2022.03.025.
Wang, Q., Hao, F., Xu, C.G., Zou, H.Y., 2020. Paleolimnological environments and the formation of high quality source rocks in the Bohai Bay Basin: an integrated geochemical study of biomarkers, stable carbon and oxygen isotopes, and trace elements. J. Pet. Sci. Eng. 195, 107753. https://doi.org/10.1016/j.petrol.2020.107753.
Wignall, P.B., Twitchett, R.J., 1996. Oceanic anoxia and the end Permian mass extinction. Science 272 (5265), 1155–1158. https://doi.org/10.1126/science.272.5265.1155.
Wu, J., Liang, C., Yang, R.C., Xie, J., 2022. Sequence stratigraphic control on the variations of organic matter in Eocene lacustrine shales within the Dongying Depression, Eastern China. J. Asian Earth Sci. 237, 105353. https://doi.org/10.1016/j.jseaes.2022.105353.
Xiong, G.Q., Jiang, X.S., Cao, X.Y., Wu, H., 2010. The characteristics of trace element and REE geochemistry of the Cretaceous mudrocks and shales from southern Tibet and its analysis of redox condition. Adv. Earth Sci. 25 (7), 730–745. https://doi.org/10.11867/j.issn.1001-8166.2010.07.0730.
Xu, J.J., Jin, Q., Xu, X.D., Cheng, F.Q., Hu, C.H., Wang, B., Chen, T., 2021. Factors controlling organic-rich shale development in the liushagang formation, weixinan sag, beibu Gulf basin: implications of structural activity and the depositional environment. Petrol. Sci. 18 (4), 1011–1020. https://doi.org/10.1016/j.petsci.2020.08.001.
Yamamoto, K., 1987. Geochemical characteristics and depositional environments of cherts and associated rocks in the Franciscan and Shimanto terranes. Sediment. Geol. 52 (1–2), 65–108. https://doi.org/10.1016/0037-0738(87)90017-0.
Yang, G.Q., Zeng, J.H., Qiao, J.C., Liu, Y.Z., Cao, W.F., Wang, C.Y., Geng, F., Wei, W.F., 2022. Differences between laminated and massive shales in the permian Lucaogou Formation: insights into the paleoenvironment, petrology, organic matter, and microstructure. ACS Earth Space Chem. 6 (10), 2530–2551. https://doi.org/10.1021/acsearthspacechem.2c00245.
Yang, J.Q., Zhang, J.T., He, Z.L., Zhang, T., 2023. Paleoenvironment reconstruction of the middle ordovician thick carbonate from western Ordos Basin, China. Petrol. Sci. 20 (1), 48–59. https://doi.org/10.1016/j.petsci.2022.08.027.
Yang, Y., Gao, F.H., Pu, X.G., Chen, C.W., Xu, W.L., 2013. Changes to depositional palaeoenvironments within the Qikou depression (Bohaiwan Basin, China): carbon and oxygen isotopes in lacustrine carbonates of the Palaeogene Shahejie Formation. Int. Geol. Rev. 55 (15), 1909–1921. https://doi.org/10.1080/00206814.2013.805926.
Zhang, K., Li, Z., Jiang, S., Jiang, Z.X., Wen, M., Jia, C.Z., Song, Y., Liu, W.W., Huang, Y.Z., Xie, X.L., Liu, T.L., Wang, P.F., Shan, C.A., Wu, Y.H., 2018. Comparative analysis of the siliceous source and organic matter enrichment mechanism of the upper Ordovician–Lower silurian shale in the upper-lower yangtze area. Minerals 8, 283. https://doi.org/10.3390/min8070283.
Zhang, L.C., Xiao, D.S., Lu, S.F., Jiang, S., Lu, S.D., 2019. Effect of sedimentary environment on the formation of organic-rich marine shale: insights from major/trace elements and shale composition. Int. J. Coal Geol. 204, 34–50. https://doi.org/10.1016/j.coal.2019.01.014.
Zhang, L.F., Dong, D.Z., Qiu, Z., Wu, C.J., Zhang, Q., Wang, Y.M., Liu, D.X., Deng, Z., Zhou, S.W., Pan, S.Q., 2021. Sedimentology and geochemistry of Carboniferous-Permian marine-continental transitional shales in the eastern Ordos Basin, North China. Palaeogeogr. Palaeoclimatol. Palaeoecol. 571, 110389. https://doi.org/10.1016/j.palaeo.2021.110389.
Zhu, G.Y., Zhang, S.C., Jin, Q., Dai, J.X., Zhang, L.Y., Li, J., 2005. Origin of the Neogene shallow gas accumulations in the Jiyang superdepression, Bohai Bay Basin. Org. Geochem. 36, 1650–1663. https://doi.org/10.1016/j.orggeochem.2005.08.009.
Zhu, X.M., Zhang, M.Z., Zhu, S.F., Dong, Y.L., Li, C., Bi, Y.Q., Ma, L.C., 2022. Shale lithofacies and sedimentary environment of the third member, Shahejie Formation, Zhanhua sag, eastern China. Acta Geol. Sin.-Engl. Ed. 96 (3), 1024–1040. https://doi.org/10.1111/1755-6724.14804.
Zou, C.N., Yang, Z., Zhu, R.K., Wu, S.T., Fu, J.H., Lei, D.W., Hou, L.H., Lin, S.H., Pan, S.Q., 2019. Geologic significance and optimization technique of sweet spots in unconventional shale systems. J. Asian Earth Sci. 178, 3–19. https://doi.org/10.1016/j.jseaes.2018.07.005.